Master's thesis

NTNU
Norwegian University of Science and Technology
Faculty of Engineering
Department of Energy and Process Engineering

Kristine Midtbø

CFD modelling of mixing in a small-scale UASB biogas reactor

Master's thesis in Energy and Environmental Engineering
Supervisor: Kristian Myklebust Lien (NTNU)
Co-supervisor: Knut Vågsæther (USN)
June 2022

NTNU
Norwegian University of Science and Technology

TELEMARK TECHNOLOGIES™

Kristine Midtbø

CFD modelling of mixing in a small-scale UASB biogas reactor

Master's thesis in Energy and Environmental Engineering
Supervisor: Kristian Myklebust Lien (NTNU)
Co-supervisor: Knut Vågsæther (USN)
June 2022

Norwegian University of Science and Technology
Faculty of Engineering
Department of Energy and Process Engineering

Project description

The thesis will use CFD to approach mixing in a UASB biogas reactor called Telemarksreaktoren. The aim shall be to produce results of industrial interest by investigating how mixing in the reactor may be linked to the biogas yield. The specialization project within the same subject conducted by the author of this thesis in the autumn semester of 2021 shall be used as a foundation for the work of the thesis. The models from the specialization project will be used as a basis to conduct transient simulations of Telemarksreaktoren to understand how new substrate is inserted and mixed in the biogas tank. Particle injection simulations, 3D simulations, and other methods for approaching mixing should be considered during the thesis work. The mixing shall further be linked to the biogas production and discussed with the frame of increased biogas yield to provide the industry with recommendations concerning improvements for the mixing in Telemarksreaktoren.

Abstract

The aim of this thesis is to understand how the incoming substrate is mixed in Telemarksreaktoren (TR) using computational fluid dynamics (CFD) simulations for the purpose of finding recommendations for improving the mixing in TR. This objective seeks to determine whether enhancing the mixing in TR can increase the biogas yield from reactors. Biogas is a growing sector that not only generates renewable energy in the form of methane-containing gas but also decreases atmospheric methane emissions. Effective biogas reactors are thus attractive not just due to their capacity to decrease greenhouse gas emissions, but also due to the value of the biogas itself. This thesis will address the mixing of new substrate based on a theory for the proliferation of incoming particles throughout the volume to be crucial for effective gas production. The problem will be resolved by running transient 2D axisymmetric simulations of the incoming substrate with the use of ANSYS Fluent. A case study was conducted to determine how velocity and geometric characteristics at the inlet affect the flow pattern prior to conducting simulations of a recirculation pump. To provide results for discussing the anticipated exploitation of biogas potential, a two-phase flow is conducted to validate the findings and investigate the particle distribution. The simulation of the case study revealed a not fully developed flow, indicating unutilized mixing potential. Simulations of particles revealed implementation of a recirculation pump to increase the disperse of the incoming substrate. High velocity and simple geometry were thus determined to be preferable, and a recirculation pump was decided to be advantageous whenever mixing is to be enhanced.

Sammendrag

Denne avhandlingen tar for seg hvordan innkommende substrat mikses i Telemarksreaktoren (TR) ved å bruke numerisk fluiddynamikk (CFD) til å simulere forskjellige strømningsmønstre i reaktoren slik at miksingen kan forbedres. Dette gjøres for å finne generelle anbefalinger for geometri og oppsett av reaktoren som kan gi økt biogassutbytte. Biogassindustrien er i dag voksende over hele verden. Noe av årsaken kan være evnen til å produsere fornybar energi i form av en metanholdig gass samtidig som metangassutslipp til atmosfæren reduseres. Dette resulterer i at effektiv produksjon av biogass både reduserer utslipp av klimagasser og er en verdifull energikilde. Ettersom spredningen av innkommende partikler har vist seg å være viktig for effektiviteten til en biogassreaktor vil dette være fokusområdet til denne avhandlingen. Gjennom 2D transient aksesymmetrisk simulering av innpumpingen av substrat i TR vil miksingen modelleres i ANSYS Fluent. Først vil en case-studie bli gjennomført for å undersøke hvordan hastighet og geometri ved innløpet påvirket miksingen. Videre vil en resirkuleringspumpe bli modellert i systemet for å se om dette kunne forbedre innpumpingen. Til slutt vil systemet bli simulert med tofase for å observere hvordan innkommende partikler fordeles i volumet ved innpumping. Partikkelsimuleringene vil gjennomført bli for å kartlegge om det var grunn til å tro at det fantes en mer effektiv metode for å øke hastigheten på nedbrytningen av nytt substrat. Case-studien viste at strømningene i tanken ikke var fullt utviklet. Dette impliserte at effektiviteten til reaktoren sannsynligvis kunne økes ved å optimalisere miksingen. Partikkelsimuleringene viste videre at ved bruk av en resirkuleringspumpe ville partiklene distribueres over et større volum. Dermed ble det konkludert med at en enkel geometri i kombinasjon med høy hastighet ved innløpet var å foretrekke, men at en resirkuleringspumpe ville være nødvendig dersom miksingen skulle forbedres merkbart.

Contents

List of Figures

List of Tables

1 Introduction

1.1 Background and motivation

Anaerobic treatment of biological wastewater is a field of environmentally sustainable technology critical to reaching Goal 6 and Goal 7 of the United Nations 2030 Sustainable Development Agenda [1]. The reason is the ability anaerobic wastewater treatment has considering carbon footprint, excess sludge production, and biogas recovery when compared to aerobic solutions. Goal 6 aims to "*Ensure availability and sustainable management of water and sanitation for all*" [1]. Due to the low construction and operating cost of anaerobic technology, the technology to reach goal 6 will be within reach in most parts of the world [2]. This is also an important aspect of goal 7, which aims to "*Ensure access to affordable, reliable, sustainable and modern energy for all*" [1]. With the use of the energy from biogas production, both more sustainable wastewater treatment and a low carbon footprint will be possible.

The upflow anaerobic sludge blanket (UASB) reactor is one of the most common high-rate anaerobic wastewater treatment methods [3]. The reactors are compact and effective because they can use a high rate of wastewater in the process. The effective treatment is due to the formation of granules containing organic digestive microorganisms [4]. These granules are added or formed during start-up of a UASB reactor and will be maintained through normal operating conditions. The granules are dense and compact, which results in their settling in the reactor's tank. This contrasts with flocculant sludge, which has less advantageous settling properties [2]. Furthermore, the granules become more resistant to toxins and shocks in the process. This is due to the limited diffusion within the granules [5]. However, the granules and the digestive microorganisms are sensitive to changes in for example temperature and pH [6]. The mixing pattern of the incoming substrate is therefore critical to ensure effective and optimal operating conditions for the granules [2].

Mixing in UASB reactors aims to provide the microorganisms with new organic substrate for digestion as well as provide a uniform temperature in the tank. Mixing can be achieved using mechanical, hydraulic, and pneumatic techniques. The techniques further vary from continuously to intermittently mixed reactors, where the frequency may have a period varying from minutes to hours. The choice of mixing method depends on several factors. Usually, the frequency determined by the settling qualities and the energy demand, while the techniques are usually chosen to benefit the geometry of the tank. As a result, understanding the hydraulics in a tank has become critical to ensuring appropriate substrate distribution and uniform temperature distribution. [6]

Computational fluid dynamics (CFD) is frequently used as a method to understand the complex hydraulics in a UASB reactor. The opaqueness of the sludge makes experimental methods challenging [7]. The sludge can then be simulated using one-, two-, or three-phase simulations, depending on the problem. In order to reduce computational costs, this approach frequently ignores biochemical reactions. Another reason for using CFD when modelling is the high cost of building and operating large-scale test reactors. CFD is then regarded as a low-cost method to gather information. In addition, to compare various geometries and solutions in order to optimize the design is considered relatively effortless when using CFD as a modelling method.

This thesis will use CFD to investigate the geometry of the UASB reactor Telemarksreaktoren (TR) in order to understand how the geometry and physical variables at the inlet influence the mixing of new substrate in the tank. TR employs periodic hydraulic mixing by flushing new substrate into the cylindrical tank's floor center. The flushing period is determined by the substrate's accessibility and the required hydraulic retention time (HRT). The aim of this is to understand how mixing changes as geometric configurations and the conditions at the inlet change. This is significant because the TR system is still under development, and mixing is critical when optimizing a biogas reactor [6]. For simplicity, the geometry of the tank will be simplified to achieve axis symmetry, and the fluid will be simplified to a Newtonian incompressible fluid. The majority of the analysis will use water as the fluid in the tank, but a two-phase flow with particles in water will also be considered. The thesis is based on work completed by the author during the autumn semester of 2021 at the Norwegian University of Science and Technology (NTNU).

Previous work

As previously stated, this thesis is based on a project conducted by the author at NTNU during the autumn semester of 2021. The objective of this work was to use ANSYS Fluent to characterize the low mixing zones of TR in order to do a CFD study in the reactor tank [8]. The simulations in this project were steady-state simulations using water as a fluid. With an inlet velocity of $0.2\,\mathrm{ms}^{-1}$ and the simplified geometry, the lower third of the tank was found to be the area of mixing. However, the model uncertainty was significant, therefore transient simulations with particles were advised as further research to better understand the mixing conditions.

To obtain a steady state solution for the flow in the system, $k-\epsilon$ SST was used to model the turbulence. The model was determined to be appropriate for the system with an inlet turbulence intensity of 5%, a grid size of $h = 3\,\mathrm{mm}$, residual criteria of 10^{-5}, and 6000 iterations. The resulting flow field and flow zones of TR are presented in Figure 1 and Figure 2 respectively.

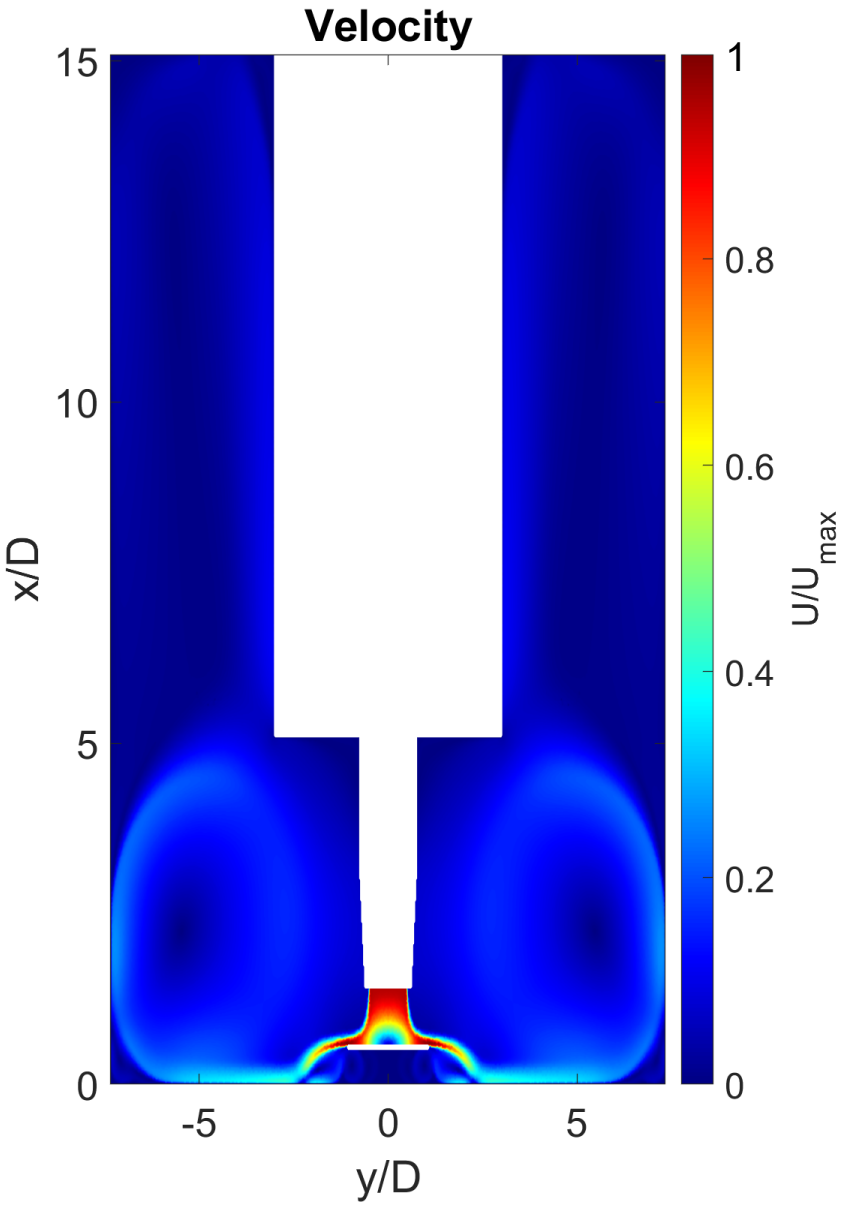

Figure 1: Plot of the velocity magnitude of TR from a steady-state simulation. U_{max} is denoting the inlet velocity and D is the diameter of the inlet.

Source: [8]

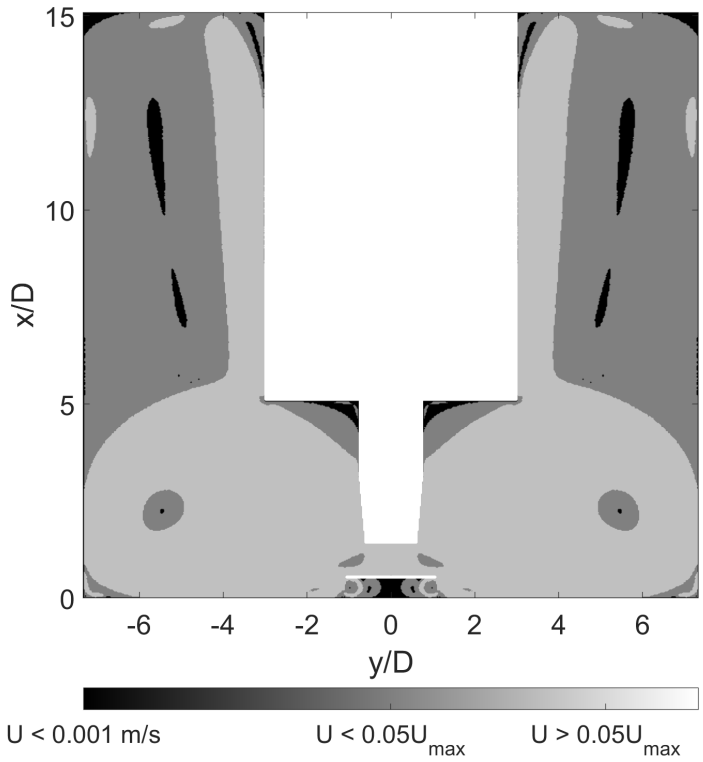

Figure 2: Plot of the flow zones of TR from a steady-state simulation. U_{max} is denoting the inlet velocity and D is the diameter of the inlet.

Source: [8]

The findings of this study demonstrated mixing to be more likely to occur in the bottom third of TR. There were various vortex formations in this volume, i.e., a large vortex forming close to the wall and smaller vortices found around the plate's edge. The simulations, however, were steady-state and did not address multi-phase or 3D effects. These are substantial uncertainty, yet they are the only outcomes involving mixing in TR. In other words, even though knowledge in this area is limited, there are some trends to anticipate for the mixing pattern of TR.

The model for this project is verified but not validated, and the main discussion concerning errors and uncertainties will now be presented. The discretization error was minimized by a convergence analysis of different meshes, where $h = 3\,\text{mm}$ was found to be sufficient. Further, the turbulence model was found to predict the trends of the flow, but only the averaged velocity field will be modelled due to the choice of a RANS model. The turbulent fluctuations are consequently not modeled, but the model is accepted given a lack of experimental validation data. The application uncertainties, together with the simplifications for the fluid and geometry, were considered the largest source of error in this project. The fluid simplification from non-Newtonian multi-phase manure to Newtonian single-phase water has in some situations been shown in the literature to be an invalid simplification [9]. However, the simplification was considered necessary to obtain some results concerning the flow zones of TR within the given time. The geometry was also simplified by neglecting the effect of the particle retention devices, supporting leg, and the free surface of the gas stored in the tank. Due to these simplifications, it was determined that the solution for the top portion of the reactor had a significant degree of uncertainty. However, due to the computational cost for a full 3D model, a 2D axisymmetric setup was still preferred. Another argument for accepting the model was no experimental data for the flow causing the solution to be uncertain despite an exact geometric model. Thus, the TR model was acknowledged for simulating the principal flow effects to an extent deemed suitable for engineering applications.

1.2 Scope of the thesis

The aim of this thesis is to understand how the incoming substrate is mixed in TR using ANSYS Fluent to perform CFD simulations for the purpose of finding recommendations for improving the mixing in TR. Transient 2D simulations based on the project setup described in section 1.1 will be determining how the flow quantities and geometrical changes influence mixing. A case study will be used to illustrate the effect of different inlet configurations. In addition, a recirculation pump is modelled to assess whether its inclusion in the system to promote mixing would be beneficial. Finally, particle simulations will be conducted to determine whether the particle distribution may reveal configurations having a potentially higher biogas yield. Due to a lack of information and the unavailability of test plants, the measurement of enhanced biogas output is judged outside the scope of this thesis. For the same reason, the results will not be validated against experimental data, but the model will be calibrated and discussed. Simulations in three dimensions are deemed out of scope. This is due to the institute-allotted time for completing the thesis, as well as the decision to aim for results of high industrial interest.

1.3 Outline of the thesis

This thesis is written for Telemark Technologies (TT) and therefore seeks to provide industry-relevant results. However, there are sections of this thesis that are less relevant to the industry because they describe the methods used to obtain the results. On the other hand, this is crucial information in the event that TT wishes to apply a similar strategy to future versions of their reactor.

First, the thesis will introduce the required theory for discussing the methods and results. The section contains fundamental information regarding biogas production, the used reactor, and models of turbulence and particle flow. The last subsection is intended to provide the reader with information regarding verification and validation in the field of CFD.

The objective of the methodology section is to provide the reader with the information necessary to reproduce the results of this thesis. This section is written with rather specialized technical terminology because it assumingly will be of interest to readers in possession of prior knowledge of CFD. This section provides details regarding the computational domain, mesh, simulation setup, initial and boundary conditions, and models employed. In addition, the sections are organized in chronological order to provide the reader with insight into the process of investigating the mixing of TR. The first section describes the method used to calibrate the transient flow, followed by a case study. Prior to describing the setup for particle simulations, the procedure for simulations of recirculation pumps is presented.

The purpose of the result section is to describe and present the findings of the simulations described in the method section. To facilitate the reader's navigation through the results, this section is divided into subsections based on the methodology. This causes findings of industrial and academic importance to be presented in the same section. However, all results will be commented on and described to guide the reader through the indications of the results.

The discussion section will first consider the limitations of the thesis's scope, before the methods and numerics are discussed. Lastly, a discussion of the results in the context of practical applications will be presented. The purpose of the discussion is to explain both the strengths and weaknesses of the methods, solutions, and results presented in the thesis. The discussion is divided because, from an industrial standpoint, the discussion of the results and their practical applications is the most interesting portion. However, the discussion of methods and numerics is essential because it addresses the reliability of the obtained results.

The last sections of this thesis aim to conclude and give suggestions for future studies regarding mixing in TR. The purpose of the conclusion is to bring the thesis to a close by offering recommendations for the development of mixing in TR. Lastly, thoughts for future work are presented with the aim of suggesting some practical studies to confirm the trends found in this thesis's work.

2 Theory

2.1 Biogas and UASB reactors

Biogas is a gas mixture primarily consisting of 50%-75% methane, 25%-50% carbon dioxide, and a small fraction of other gases such as hydrogen sulfide, ammonia, and water vapor. Because of the similarities between natural gas and biogas, biogas is regarded as an important substitute for natural gas in terms of lowering carbon dioxide emissions. Biogas is produced from anaerobically decomposed organic material and is thus a renewable energy source. The decomposition process is frequently described as a four-step cascade decomposing large-scale molecules into methane and carbon dioxide. The four steps of the cascade are described as: hydrolysis, acidogenesis, acetogenesis, and methanogenesis, and are depicted in Figure 3. [10]

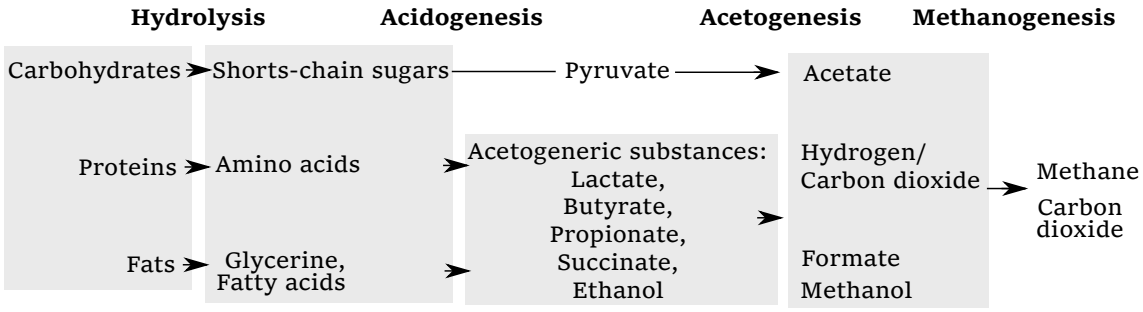

Figure 3: Four-step cascade of bioreactions to produce biogas anaerobically from organic materials.

During the biogas production process, the four cascading steps of anaerobic digestion (AD) will occur simultaneously. As a result, the various cascades are presented, beginning with the process of digesting long-chain organic material and progressing to the process of digesting shorter molecules. The first step in the cascade is known as hydrolysis. Carbohydrates are hydrolyzed into short-chain sugars; fats into glycerin and fatty acids; and proteins into amino acids. Acidogenesis is the second step in the cascade. This is the stage at which the hydrolytic phase's monomers are broken down into short-chain organic acids. Acetogenesis is the third cascade step. In this step, the organic acids are reduced to formate and acetate. In the fourth and final step, methanogenesis, methane and carbon dioxide are formed. The cascade is driven by several groups of bacteria and archaea, and the efficiency of the microorganisms is influenced by their environment. [11]

Temperature, pH, retention time, organic loading, and mixing are some of the important factors influencing the effectiveness of the microorganisms [6]. The temperature range in the reactors depends on the tolerance of the microorganisms. Psychrophilic microorganisms may produce biogas at a temperature of 4-25 °C, while extremophilic microorganisms can produce biogas at temperatures exceeding 65 °C. On the other hand, the temperature of a reactor is often decided by a trade-off between energy consumption and production. High temperatures will increase the reaction rate, but consequently increase the energy consumption as well. This is the reason for mesofilic (30-40 °C) and thermophilic (50-60 °C) to be the most common temperature ranges in AD [12]. pH is an important and sensitive factor in AD. A 0.5 pH change can cause a significant change in microbial metabolism, influencing reaction kinetics and biogas yield [6]. Due to the highly sensitive methanogens, the optimal pH for AD is near 7. In the event of pH below 6.3 or above 7.8, the process may fail [6]. Retention time refers both to the solid retention time (SRT) and the hydraulic retention time (HRT). SRT denotes the retention time of the microbial culture in the digester, while HRT is the retention time of the liquid phase. The HRT is defined as the ratio between reactor volume and the flow rate of the influent. Depending on the rate of digestion, the HRT will vary with the choice of reactor configuration. Usually, an HRT of between 10 and 25 days will be suitable, but both higher and lower HRT may be optimal. The organic load rate (OLR) is the amount of raw material added to the reactor per day per unit volume and is to be expressed as the ratio between the feed concentration and the HRT. It is also important how this organic load is distributed throughout the reactor volume, i.e., the mixing of the incoming substrate in the

reactor. [6]

The aim of mixing in AD is to promote contact between the microorganisms, substrates, and nutrients while also assuring uniform temperature distribution throughout the tank [6]. This is the reason well mixed reactors generally have an increased biogas yield compared to those with no mixing [13]. It is, therefore, crucial when designing a biogas reactor to address mixing. Mixing can be accomplished by employing pneumatic, hydraulic, and mechanical techniques at different intensities and frequencies. The choice of mixing technique depends on the reactor type and the type of influent, as well as the energy available. Continuous mixing in full-scale AD can consume up to 50% of the entire plant's energy consumption. Intermittent mixing will therefore reduce the energy expenditure of the plant. However, the opaqueness of the sludge often makes it hard to measure the mixing of a tank [7]. To ensure adequate mixing when designing a reactor, modeling methods such as CFD are used.

UASB reactors

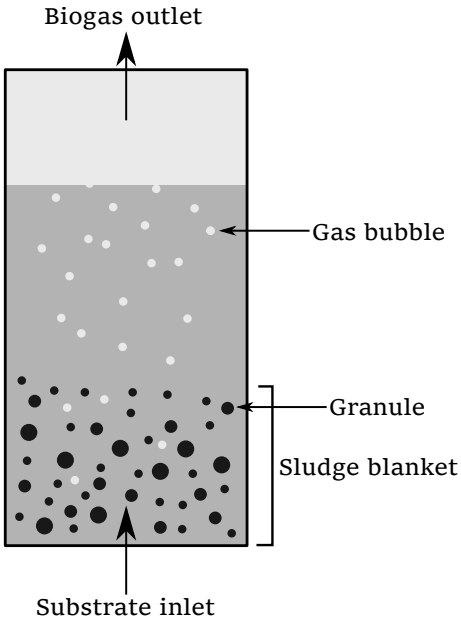

Figure 4: System sketch showing how the influent is flushed through the sludge blanket in an Upflow anaerobic sludge balnket (UASB) reactor.

Upflow anaerobic sludge blanket (UASB) reactors are characterized by the inlet flow flushing through a sludge blanket of granules. Granules may be described as aggregates of microorganisms collected in particles. The density of the granules is somewhat increased compared to the surrounding fluid, therefore, a sludge blanket is usually found in the lower part of a UASB tank as illustrated in Figure 4. The inlet of these tanks is placed below the sludge blanket to effectively spread the incoming substrate through the sludge blanket. The gas is further collected in the tank's upper section and transported for use outside of the digestion tank.

The granules are particles with digestive microorganisms. First, the gas forms on the inside of the particle in small internal pores. Gas production is a transient process affected by the granule size and access to organic substrate, as well as the temperature, pH, and pressure of the surrounding environment. This gas production decreases the density of the particles as a function of the produced gas. When the internal pores are filled with gas, the produced gas will escape through a channel in the granule. This causes a gas bubble to form at the surface of the granule. When the gas bubble is sufficiently large, the bubble will escape the granule. Because the density of the granule is only slightly increased compared to the surrounding fluid, the bubble formation at the surface will often cause the granules to rise like raisins in soda.[14]

Based on the geometry and substrate, the method for mixing new substrate into the volume of a UASB reactor may vary. Because most of the digestive culture is within the granules, the mixing in such reactors aims to distribute the new substrate while also preventing washout of granules [15]. To describe the mixing in a reactor, mixing zones are frequently used in literature [16]. *Poorly mixed zones* were defined by Karim as areas with a velocity of less than 5% of the peak velocity, while a *dead zone* was defined by Wu as an area with velocities less than $0.001\,\mathrm{ms}^{-1}$ [16]. Numerous studies have shown that reducing the size of these zones increase biogas production [16]. Mixing is thus enhanced by minimizing these low-velocity zones. However, to describe the mixing of a UASB reactor, both mechanical mixing and the granule dynamics need to be addressed. Because the velocity of the granules influences the mixing process in a UASB reactor, the process is difficult to describe. As a result, the problem is frequently divided into two different perspectives. The first perspective is the forced mixing, either by pneumatic, hydraulic, or mechanical techniques, or by the incoming substrate. The second perspective is the

motion of the granules. This often includes their density, terminal velocity, size, shape, and ability to produce gas. However, the forced mixing will affect the motion of the granules, and the granules will affect the flow pattern in the mixing. Therefore, reactor tanks are often modeled before pilot or scale models are built.

2.2 Telemarksreaktoren

Telemarksreaktoren (TR) is a patented baffled UASB reactor designed for biogas production at medium- to large-scale farms in Norway. Yara, the University of South-Eastern Norway (USN), and Telemark Technologies (TT) are the owners of the patent in Norway, where TT is responsible for the manufacture and sale of the reactors. TR was designed to handle manure as a substrate, but has also been shown to work with organic waste and wastewater. The total solid (TS) content of the substrate should not exceed 10%, with a TS content of close to 4% yielding the best results. TR operates in a mesophilic environment and for pig manure of 4% TS, the biogas production has been shown to be effective for HRT larger than 17 hours [17].

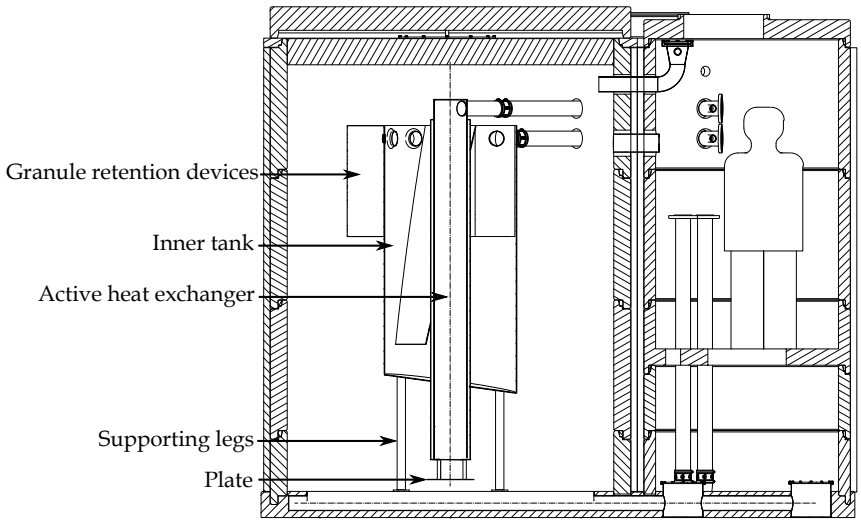

Figure 5: Drawing of Telemarksreaktoren showing some of the components of the main tank.

Figure 5 shows the main parts of the AD tank through a plane in the center of TR. Before flushing the substrate into the tank, the substrate is heated by the active heat exchanger until a temperature of approximately 38 °C is reached. The plate at the heat exchanger's outlet serves as a stagnation plate, distributing new substrate throughout the tank while protecting a screwer installation mounted at the floor of TR. This screwer installation serves the purpose of preventing settling of heavy particles in the tank. Several granule retention devices are distributed on the outside of the inner tank to constrain the motion of the granules forming during the process. The granule retention devices are parts of the baffle configuration, along with the baffle wall inside of the inner tank. The floor of the inner tank is tilted to make draining of the tank during shutdown of the plant simple.

A passive heat exchanger is included in the system of TR to ensure effective energy consumption. In this concentric parallel flow exchanger, the digested substrate transfers heat to the entering substrate. In addition, the active heat exchanger and heat cables inside the main tank aim to keep the temperature stable for mesophilic conditions. It is vital that the substrate is properly mixed in order to keep the temperature gradients in the tank modest.

The UASB principles of TR are illustrated in Figure 6, where the influent is flushed from the heat exchanger into the granule bed with a given frequency. This flushing activates the movements of the system where the substrate passes through particle retention devices before entering the inner tank. The substrate will then be pushed farther around the baffle wall and out of the tank by using another particle retention mechanism. This baffle motion, together with the particle retention devices, is meant to keep the tank's culture balanced and effective by limiting granule washout. Furthermore, the digested substrate will pass through the passive heat exchanger before being preserved on the exterior of the TR system.

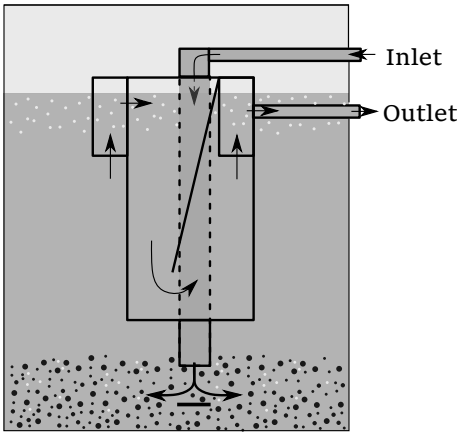

Figure 6: System diagram showing how Telemarksreaktoren uses the UASB principles.

Because TR is in the pilot stage of development, there has been some empirical experience with the reactor's operation. Managing the flow of manure through the system has been the most difficult component of the TR. Pipes with insufficient diameters or severe bends appear to gather solids, resulting in reactor downtime. This has also been a problem with the exit of the active heat exchanger. To prevent particles from settling inside the active heat exchanger, the pumping frequency has been reduced. However, the frequency is limited by the HRT and the effectiveness of the heat exchangers. As a result, it is important to look into whether a geometry alteration might assist in preventing heat exchanger plug sedimentation. This can be accomplished by extending the distance between the exchanger's outlet and the first stagnation point, or by including a recycling pump into the system. Given these parameters, the simplest geometries have been demonstrated to perform better over time.

The operating expertise gathered for the system of TR is mostly derived from an early stage pilot at *Tvedestrand og Åmli videregående skole*. The geometry of the pilot differs slightly from the system investigated in this thesis. The experience with the operating situation is still interesting and crucial for the system's development. Together with the project detailed in section 1.1, the expertise from this pilot plant serves as the foundation for understanding how TR is functioning today.

2.3 Governing equations

This subsection intends to provide the mathematical background for characterizing a flow field. The conservation of mass and momentum will be required to explain a physical system given any arbitrary flow. According to the conservation laws of physics, mass and energy never disappear or emerge. This section's equations constitute the system of equations that must be solved to describe any arbitrary flow. Simplifying assumptions will be given via the derivation of equations to offer information on the limitations acquired.

Conservation of mass

Given any arbitrary control volume, V, the rate of the increased mass inside V is equal to the net mass flow through a closed surface, S, containing V. Given the surface normal of the closed surface, $\mathbf{n}$, the velocity field of the mass, $\mathbf{U}$, a time scale, t, and the density of the moving mass, ρ, may this be mathematically written as

$$\frac{\partial}{\partial t}\int_V \rho dV = -\oiint_S \rho \mathbf{U}\cdot\mathbf{n}dS \tag{1}$$

The conservation of mass is thus expressed as Equation 1, assuming no mass creation or annihilation within V. The Divergence theorem may be applied to Equation 1 because of the assumption of

the equation to be valid for any arbitrary volume. The differential form of conservation of mass can then be written as

$$\frac{\partial \rho}{\partial t} + \frac{\partial}{\partial x_i}(\rho u_i) = 0 \tag{2}$$

where u_i is the i-th velocity in the x_i direction. For incompressible flows, i.e., flows with constant values for ρ, may Equation 2 be simplified to

$$\frac{\partial u_i}{\partial x_i} = 0 \tag{3}$$

Equation 3 is in this form often referred to as the continuity equation.

Momentum equations

The momentum balance on a stationary volume is given by the forces acting on the volume. The pressure field, p, on the volume results in a pressure force and the viscous shear stress, τ, results in viscous forces. Together with other external volume forces, $\mathbf{f}$, may the momentum balance for V be written as

$$\int_V \frac{\partial \rho \mathbf{U}}{\partial t} dV + \int_S \rho \mathbf{U}\mathbf{U} \cdot \mathbf{n} dA = -\int_S p\mathbf{n} dA + \int_S \tau \cdot \mathbf{n} dA + \int_V \rho \mathbf{f} dV \tag{4}$$

When the fluid inside V is an incompressible Newtonian fluid , i.e., a fluid of constant viscosity and density, the momentum equation in Equation 4 is often simplified to the Navier-Stokes equation on a differential form given by

$$\frac{\partial u_i}{\partial t} + u_j \frac{\partial u_i}{\partial x_j} = -\frac{1}{\rho}\frac{\partial p}{\partial x_i} + \nu \frac{\partial^2 u_i}{\partial x_j \partial x_j} + \frac{f_i}{\rho} \tag{5}$$

where f_i is the forces acting on the fluid in the i-th direction.

2.4 Turbulence models

Turbulence modeling is a method for simulating the mechanics of turbulence in a flow. The idea of turbulence models are often derived from the turbulent energy cascade. The energy cascade is usually divided in three scales: the energy containing range, the internal range, and the dissipation range. The energy containing range is often referred to as the integral scale where the turbulent kinetic energy is produced. The internal range is the range dominated by energy transfer. The dissipation range is further the smallest scales of the cascade dominated by dissipation of energy. The characteristics of these regions is further used to find a characteristic length scale, velocity scale, and time scale describing the specifics of a turbulent flow. In CFD modeling of such flows, the mesh and time step sizes must be fine enough to capture the small-scale physics, yet the domain must be wide enough to catch large-scale movements. As a result, the mesh usually has a large number of cells and the temporal discretization results in a small timestep.

Direct numerical simulations (DNS) are the method of directly solving the Navier-Stokes equations. Small-scale eddies are typically modeled because these simulations require a significant amount of processing resources. When small-scale eddies are modeled, the model is characterized as a large eddy simulation (LES). Because LES solves Navier-Stokes equations for large-scale eddies, the requirement for finer mesh is reduced compared to DNS, as is the demand for computational power. Large domains, on the other hand, will increase the cost of LES. The Reynolds-Averaged Navier-Stokes (RANS) equations can be solved as a third alternative. RANS solves the Navier-Stokes equations for mean flow parameters, focusing on the impacts of turbulence rather than exact modelling of the turbulent scales. By Reynolds-averaging Equation 5 will the RANS equations be given by

$$\frac{\partial U_i}{\partial t} + U_j \frac{\partial U_i}{\partial x_j} = -\frac{1}{\rho}\frac{\partial P}{\partial x_i} + \nu \frac{\partial^2 U_i}{\partial x_i \partial x_j} - \frac{\partial \overline{u_i' u_j'}}{\partial x_j} + \frac{F_i}{\rho} \tag{6}$$

where U_i denotes the averaged velocity of u_i, u_i' the turbulent fluctuations defined as the difference between U_i and u_i, ν denotes the kinematic viscosity, and F_i denotes the average of f_i. The second last term on the right hand side of Equation 6 can further be written as

$$\frac{\partial \overline{u_i' u_j'}}{\partial x_j} = \frac{1}{\rho} \frac{\partial \rho \overline{u_i' u_j'}}{\partial x_j} \tag{7}$$

where $\rho \overline{u_i' u_j'}$ in Equation 7 then represents the Reynolds stress. The continuity equation in Equation 3 and RANS equations in Equation 6 describe the motion of a fluid inside of V. However, this set of four equations usually contain more than four unknowns. In order to solve the set of equations is often a turbulence model used to address this problem.

The Boussinesq approximation hypothesis states the Reynolds stress tensor to be proportional to the mean strain rate tensor, i.e.,

$$\rho \overline{u_i' u_j'} = \rho \frac{1}{3} \overline{u_i' u_j'} \delta_{ij} + \rho \nu_T \Big(\frac{\partial U_i}{\partial x_j} + \frac{\partial U_j}{\partial x_i} \Big) \tag{8}$$

where δ_{ij} is the Kronecker delta and ν_T is turbulent viscosity. The mean of the fluctuations squared is used to calculate the TKE in relation to the Reynolds stress. This gives the definition of k

$$k = \frac{1}{2} \overline{u_i' u_i'} \tag{9}$$

Inserting Equation 9 into Equation 8 then yields the Reynolds stress tensor to be approximated by

$$\rho \overline{u_i' u_j'} = \rho \frac{2}{3} k \delta_{ij} + \rho \nu_T \Big(\frac{\partial U_i}{\partial x_j} + \frac{\partial U_j}{\partial x_i} \Big) \tag{10}$$

Several turbulence models employ this approximation to model the Reynolds stress of a turbulent flow and thereby solve the closure problem of the RANS equations.

$k - \epsilon$ model

The $k - \epsilon$ model is a RANS model that solves the closure problem by incorporating transport equations for turbulent kinetic energy (TKE), k, and turbulent dissipation, ϵ. The integral scale is then represented by the TKE, while the dissipation in the small-scale is described by ϵ. This relates the Reynolds stresses to the mean flow characteristics. The Reynolds stress may then be expressed as the product of two times the density and the TKE. Further is the transport of TKE given by

$$\frac{\partial k}{\partial t} + U_j \frac{\partial k}{\partial x_j} = \Big[-\frac{2}{3} k \delta_{ij} + \nu \Big(\frac{\partial U_i}{\partial x_j} + \frac{\partial U_j}{\partial x_i} \Big) \Big] \frac{\partial U_j}{\partial x_j} + \Big[\Big(\nu + \frac{\nu_T}{\sigma_k} \Big) \frac{\partial k}{\partial x_j} \Big] - \epsilon \tag{11}$$

where σ_k is the turbulent Prandtl number for k and ν_T is given by

$$\nu_T = C_\nu \frac{k^2}{\epsilon} \tag{12}$$

and C_ν is a proportionality constant. The turbulent viscosity is deduced when using the Boussinesq approximation from Equation 10 for mimicking behaviour of shear stress in a flow. Further is ν_T assumed to be proportional to the product of the length and velocity scale. By dimensional analyses is these scales written in terms of k and ϵ, with no additional variables introduced into the equations. The turbulent dissipation is then both present in Equation 11 and Equation 12 meaning that the set of equations still misses one equation. The transport equation for ϵ is then given by

$$\frac{\partial \epsilon}{\partial t} + U_j \frac{\partial \epsilon}{\partial x_j} = C_{\epsilon 1} P_k \frac{\epsilon}{k} + \frac{\partial}{\partial x_j} \Big(\frac{\nu_T}{\sigma_\epsilon} \frac{\partial \epsilon}{\partial x_j} \Big) - C_{\epsilon 2} \epsilon^2 \tag{13}$$

where $C_{\epsilon 1}$ and $C_{\epsilon 2}$ are proportionality constants, σ_ϵ is the turbulent Schmidt number, and P_k is the production of TKE defined as

$$P_k = -\overline{u_i' u_j'} \frac{\partial U_i}{\partial x_j} \tag{14}$$

Equation 13 with the definition of P_k as in Equation 14 does not introduce new variables and the RANS is then a closed problem possible to solve with no further modeling.

$k-\omega$ model

Another example of a two-equation RANS model is the $k-\omega$ model. Instead of modeling the TKE and dissipation, are $k-\omega$ modeling TKE and the turbulent frequency, ω. ω may also be described as the specific dissipation rate and the definition of ω is given by

$$\omega = -\frac{\epsilon}{\beta^* k} \tag{15}$$

where β^* in Equation 15 is a positive constant. The transport equations for the $k-\omega$ model is then given by

$$\frac{\partial k}{\partial t} + U_j \frac{\partial k}{\partial x_j} = P_k + \frac{\partial}{\partial x_j}\Big[\Big(\nu + \frac{\nu_T}{\sigma_k}\Big)\frac{\partial k}{\partial x_j}\Big] - \beta^* k\omega \tag{16}$$

$$\frac{\partial \omega}{\partial t} + U_j \frac{\partial \omega}{\partial x_j} = \gamma_1\Big[2\Big(\frac{\partial U_i}{\partial x_j} + \frac{\partial U_j}{\partial x_i}\Big) - \frac{2}{3}\omega\frac{\partial U_i}{\partial x_j}\delta_{ij} + \Big] + \frac{\partial}{\partial x_j}\Big[\Big(\nu + \frac{\nu_T}{\sigma_\omega}\Big)\frac{\partial \omega}{\partial x_j}\Big] - \beta_1\omega^2 \tag{17}$$

where σ_ω, σ_k, γ_1, and β_1 in Equation 16 and Equation 17 all are empirically decided constants.

$k-\omega$ SST model

The $k-\omega$ SST model is a RANS turbulence model first introduced by Menter [18]. The idea behind this model is to use the strength of $k-\omega$ and $k-\epsilon$ to obtain a more robust method. The $k-\epsilon$ model will often face problems in the near wall region, while $k-\omega$ face problems when k and ω approaches zero. This gives that $k-\omega$ problems with free stream boundary conditions. However, the two methods complement each other. Menter therefore combines the two models through a blender function giving the $k-\omega$ shear stress transport (SST) model. The blending of the two models is further given by the eddy viscosity

$$\nu_T = \frac{k}{\omega}\frac{1}{\max\left[\frac{1}{\alpha^*}, \frac{SF_2}{a_1\omega}\right]} \tag{18}$$

where

$$F_2 = \tanh\phi_2^2, \qquad \phi_2 = \max\Big[\frac{2\sqrt{k}}{0.09\omega y}, \frac{500\mu}{\rho y^2\omega}\Big] \tag{19}$$

and y is the distance to the wall while S is the strain rate magnitude. With this definition of ν_T used in the transport equations for the $k-\omega$ model did Menter obtain better performance to a wide range of problems. However, the blending of the two models sometimes create instabilities and therefore cause weak convergence. [18]

2.5 Particle modelling

Particle modelling is a technique for simulating the behavior of particles in flows. For this kind of modelling, there are primarily two methods: Euler-Euler and Euler-Lagrange [19]. The key distinction between the two approaches is how the particle phase is handled. The Eulerian technique treats the particle phase as a continuum, which means that the particle routes are not tracked. The conservation equations are then derived through a control volume discussion similar to the one given in subsection 2.3. The Lagrangian technique, on the other hand, treats the particle phase as a discrete phase in which the pathway of each individual particle is tracked. A Lagrangian method, on the other hand, will demand higher computational power compared to an Eulerian method in the case of large number of particles. As a result, both approaches are often utilized in CFD research to model particle flows. [19]

For the Lagrangian method, the fluid phase is treated as a continuum by solving the Navier-Stokes equations from Equation 5. The placement of the particles in the system is further calculated based on the developed flow field. The momentum balance for one particle in the flow is then given by

$$\frac{d\mathbf{u}_p}{dt} = F_D(\mathbf{U} - \mathbf{u}_p) + \mathbf{g}\frac{\rho_p - \rho}{\rho_p} + \mathbf{F}_a \tag{20}$$

where $\mathbf{u}_p$ is the velocity vector for the particle, $\mathbf{g}$ is the gravitation vector, $\mathbf{F}_a$ represents additional working forces on the particle, and F_D is the inverse relaxation time. This relaxation time is further defined as

$$F_D = C_d \frac{3|\mathbf{u}_p - \mathbf{U}|}{4d_p} \frac{\rho}{\rho_p} \tag{21}$$

where C_d in Equation 21 is the drag coefficient for the particle and d_p is the particle diameter. The internal force per unit of mass balances the drag force operating on the particle, gravity and buoyancy on the particle, and possible extra forces per unit of mass, according to Equation 20. When utilizing this model in a turbulent flow represented by the RANS equations, the challenge of requiring the whole flow field solution, $\mathbf{U}$, will arise. In a random walk model, for example, this is handled by utilizing the field's TKE to estimate the fluctuations. The fluctuation of the flow is then given by

$$u_i' = \zeta \sqrt{\frac{2}{3}k} \tag{22}$$

where ζ is a Gaussian random number. Equation 22 is based on the definition of TKE given in Equation 9. Another way of handling the problem is to neglect the fluctuations and only use the averaged velocity field in the calculations. This is to be used when there is no interest in the turbulent fluctuating effects or when the fluctuations are considered neglectable.

The Stokes number, St, is a dimensionless number describing a particle's typical behavior in a flow. In other words, the Stokes number may be used to represent how close the particles paths follow the streamlines by comparing the particle's characteristic time to the flow's characteristic time. Given a flow velocity, U_0, far away form the particle, a particle with characteristic length, d_0, and relaxation time, t_0, will the Stokes number for this particle be given by

$$\mathrm{St} = \frac{t_0 U_0}{d_0}. \tag{23}$$

In Equation 23, the relaxation time is determined by the exponential decay in particle velocity caused by drag. Because of the definition of the Stokes number, $\mathrm{St} \ll 1$ will result in particle paths closely following the streamlines of the flow, whereas $\mathrm{St} \gg 1$ will result in particle pathways diverging from the streamlines of the flow. A Stokes number less than one will arise, for example, in flows with small particles of density close to the ambient fluid. Another reason for computing the Stokes number is to observe how the particles will change the flow pattern. When the Stokes number is high, the particle's path may deviate significantly from the flow due to viscosity changes in the ambient flow. In these instances, the influence of the particle must be accounted for in the governing equations of the flow. This impact will be regarded as negligible in the event of low Stokes numbers. As a result, when using CFD to solve particle fluxes, the modeling is separated into two categories: one-way and two-way coupled models.

One-way coupled models neglect the effect of particles onto the continuous fluid phase. For this reason, the fluid phase is modeled without including effects of particles before the particle paths are calculated based on the resulting flow field. There is, hence, only a need for one iteration process finding the solution to the liquid phase. It is, however, important to remember that the particles always affect the surrounding liquid, but this may, in some cases, be neglected. Low volume fractions of particles having the same density as the continuous phase, for instance, are anticipated to have a negligible effect on the flow. High volume fractions or large density deviations will cause the flow pattern to significantly change. Two-way coupled models include the motion of the particles in the governing equations for the continuous fluid phase to include such effects. For example, the extra term will be added to the momentum equation form Equation 5. This term can be expressed as

$$\frac{F_p}{\dot{m}_p \Delta t} = \sum \left(\frac{1}{F_D} (\mathbf{U} - \mathbf{u}_p) + \mathbf{F}_{other} \right) \tag{24}$$

where $\dot{m}_p$ is the mass flow rate of particles, Δt is the discrete time step for the discrete phase, and $\mathbf{F}_{other}$ has other interactional forces such as pressure gradient effects or virtual mass forces. Because the two momentum equations, one for the flow and one for the particles, are now mutually dependent on the other, an iterative process is needed to solve the problem. This is typically accomplished by solving the flow field iteratively, inserting the solution into the particle momentum

equation, and then finding a solution for $\mathbf{u}_p$ to insert back into the flow momentum equation. This iteration process is then repeated until a converged solution is found. Due to the extra iterations required for the two-coupled approach, more computational power is demanded in such simulations. It is therefore desirable to use one-way coupled simulations where this is a sufficient approximation.

2.6 Verification and validation

When discussing the dependability of CFD research, the phrases verification and validation are frequently employed. Verification is then described as the procedure to ensure the equations to be correctly solved by the program [20]. This involves, for example, ensuring the schemes used to solve the equations appropriately for the current situation or ensuring the mesh to be fine enough for the solver to capture the flow characteristics. Validation is further described as the process of validating a model to investigate the model's capability to forecast reality [20]. This is especially important for CFD models since simplifications of the problems are frequently required in order to obtain a solution. Validation will subsequently be required to ensure the simplifications to not adversely influence the solution to the point of failing to forecast reality. Validation in the field of CFD should be addressed using one of three methods: systematic comparison of credible results from other CFD research; experimental data; or comparison with algebraic solutions [20]. The relevance of validation in engineering is frequently connected to testing to find the most notable and significant flow features [20]. As a result, the boundary between calibration and validation is sometimes unclear in engineering contexts. Calibration is the process of ensuring a CFD code's ability to forecast global quantities of interest in particular geometries [20]. However, there is a distinction between the two concepts, which may be defined as the capacity to measure the true difference between reality and the computational outputs. In other words, calibration would provide a foundation for validation by assuring an accurate model for the particular problem.

Uncertainty will be addressed using a validation and verification procedure. Uncertainty may be defined as a possible shortcoming caused by lack of information. Uncertainties in CFD instances can be classified as model or application uncertainties. When model equations are employed to address a problem, model uncertainties occur. In other words, the correct solution of the model equations may not yield the properties of the real flow issue. Such uncertainties are crucial to examine because they address how the model's capability to forecast reality. All uncertainties resulting from a lack of available input data are referred to as application uncertainties. This might be specific boundary or initial conditions, or factors like density or viscosity. Based on the problem, such uncertainty may be difficult to handle. However, it is critical to properly examine the uncertainties in order to reach a dependable and trustworthy solution. [20]

There will always be errors in the final solution of a CFD modeled problem. This is caused by the use of discretization, convergence criteria, round off during computation, and software with errors. These errors are therefore classified as discretization, convergence, round-off, user, and code errors. The discrepancy between the precise solution of the model equations and the solution produced by the discretized solution of the same equations is defined as a discretization error. A discretization of the problem is frequently required since there is either no accurate solution or obtaining one is difficult. To discover a solution within an acceptable computation time, the issue is discretized in time and space. The discretization error quantifies the error caused by this discretization. The difference between the completely converged solution of the discretized equations and the approved solution is further defined as convergence error. Accepting a partially converged solution is frequently motivated by the need to reduce processing time. There is no solution to the set of discretized equations in most situations, such as the discretization of the RANS equations. In these instances, convergence is frequently relied on as an empirical criteria linked to the residuals for the equations. The most widely recognized convergence criterion is the solutions of the equations solved down to machine accuracy. Round-off errors are frequently associated with machine accuracy and are defined as the difference between the solution to the equations when no round-off is used throughout the computations and the solution produced when round-off is utilized. Because the numbers are saved in a computer, each number only has a limited number of digits stored. This will result in a round-off error, which may result in an incorrect solution in some situations. Because the solutions rely on human contact, the final two

types of mistakes are the most difficult to measure. User errors are associated with careless usage and human error, whereas code errors can be regarded as software flaws. Both of these categories are difficult to assess because it is preferable to have no such sources of error. They may, however, appear and, as a result, they must be addressed. [20]

There are different methods for verifying and validating a CFD model and, hence, minimizing the uncertainties and errors. Grid and iteration convergence analysis, sensitivity analysis, and comparison of the answer with experimental data or literature in the field are a few examples [20]. By refining the mesh, the error will decrease given a stable and consistent method [21]. In other words, when the discretized step sizes approach zero, the residuals of the discretized equation will also approach zero. This can be verified for the various numerical approaches used to discretize a problem. As a result, a refined mesh will produce a solution with less discretization error than a coarse mesh. The discretization error of the solution is minimized by refining the mesh until it no longer changes with the mesh. To assure the stability of the problem, temporal discretization is frequently used. The temporal discretization can be changed to correspond to the spatial discretization depending on the stability criteria of the numeric schemes. In most circumstances, the temporal discretization is initially modified in accordance with the Courand-Fredrich-Lewy (CFL) condition, which states

$$C = \frac{U_{max}\Delta t}{h} < 1 \tag{25}$$

where C is the courant number, Δt is the temporal discretization, and h is the spatial discretization [20]. The condition in Equation 25 is developed from a numerical study of numerous explicit numerical schemes used for time integration and is thus an essential condition for the stability of several schemes. However, when implicit schemes are utilized, the solution may be stable for a larger value of Δt than predicted by the CFL condition. As a result, the condition is occasionally confirmed in order to improve computing speed. On the other hand, a large time step may contribute to slower convergence resulting in a trade off for optimizing computational speed. Convergence errors can be managed similarly by lowering the convergence criteria and therefore increasing the number of iterations required to find a solution [20]. When comparing the solution of multiple criteria until the solution no longer changes, a solution with a minimized convergence error is obtained. In the absence of essential knowledge of problem properties, a sensitivity analysis may be utilized to evaluate the solution dependence with regard to the missing parameter [20]. The missing parameter can then be adjusted to various values within a reasonable range, and the resulting solutions can be compared to understand the parameter's influence on the system. After mesh convergence and analysis of unknown parameters have been completed, the solution may be compared to experimental data or well-established literature in the subject. When the solution is accepted and known to be close to reality, one will arrive at a valid and verified solution [20].

3 Method

This section aims to describe the methods used to obtain the results of this thesis in order to provide a basis for recreating the study. Therefore, this part is of little practical industrial significance but is required to provide the relevant information for discussing the findings' dependability. The first part will focus on describing the general setup common for all the simulations, before the calibration, the case study, the recirculation pump, and the particle flow simulations are described in detail. In Appendix A the simulation log is presented to provide insight into the progress of the simulations conducted. The subsections are further divided as described due to the progress of the thesis. The work started by finding literature suitable for calibration before calibration of the transient motion was conducted. Furthermore, the case study was set up for investigating and comparing different configurations of TR with the aim of finding concluding recommendations for the system when optimizing mixing. The case study provided the idea of introducing a recirculation pump to improve the mixing and, thus, the recirculation pump simulations were conducted. For the purpose of addressing increased gas production, particle simulations are conducted with the aim of understanding how new substrate is distributed in the tank. The details concerning the setup of these simulations are presented in the following subsections, but first, the general setup will be presented.

The geometry of TR was simplified according to the project described in section 1.1 [8]. Figure 7 shows two of the three computational domains for this thesis and represents the bottom 1.25 m of TR. The third geometry is a modification of Geometry 1 where the outlet face is extruded 1.43 m in the x-direction to model the full height of TR. The reason for not using this geometry for all the cases is that the previous project conducted discovered less mixing activity in the upper part of the reactor. To spare some computational time and power the domain of Geometry 1 and Geometry 2 were shortened as shown in Figure 7. The geometries includes two variable lengths, L and l, which will further be specified for each of the cases simulated. The plate in Geometry 2 thickens 3 mm and has a diameter 180 mm. Because the geometric simplifications were thoroughly discussed in the steady state project described in section 1.1, the geometry is only superficially discussed in this thesis.

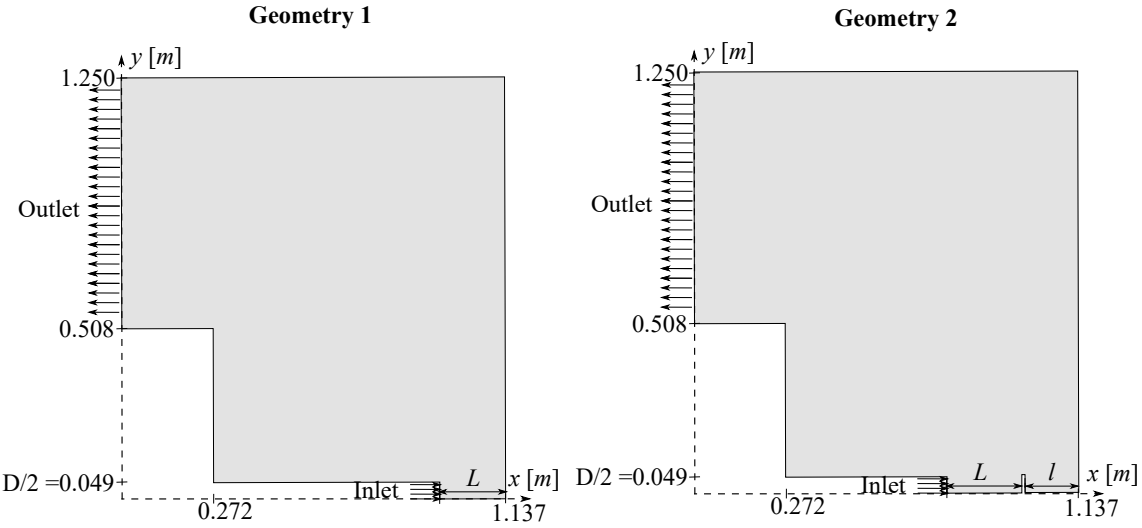

Figure 7: The computational domains used for Case 1-9. Geometry 1 was used for Case 1-6 and Geometry 2 was used for Case 7-9. L describes the distance from the inlet to the first stagnation point of the flow. l describes the distance between the floor of the tank and the elevated plate. The plate is 3 mm thick and the diameter is 180 mm.

The basis for the simulation setup is taken from the project earlier presented in section 1.1 [8]. ANSYS Fluent was used as the simulation tool, and all the cases were simulated as transient axisymmetric pressure-based problems with absolute velocity formulation. For turbulence modeling, the $k-\omega$ SST model was used, and all of the constants described in subsection 2.4 were kept as default in Fluent setup [22]. Furthermore, the boundaries of the domain were given boundary conditions; the x-axis of Figure 7 was used as the axis of rotation; the outlet was defined as a pressure outlet with a pressure profile multiplier set to 1; at the inlet, the velocity was manually set according to the case studied; the rest of the boundaries were set to be no-slip walls. The standard initialization method was used to generate an initial condition for the volume. The reference frame was then set to be relative to the cell zone, and the initial values for the setup are further specified in Table 1.

Table 1: Initial conditions for the simulations.

Gauge pressure	10 Pa
Axial velocity	0 ms^{-1}
Radial velocity	0 ms^{-1}
Turbulent kinetic energy	1 $\mathrm{m}^2\mathrm{s}^{-2}$
Specific dissipation rate	1 s^{-1}

The fluid used in the simulations was water, and all the meshes were generated with quadratic cells and a grid size of 3 mm. The residual criteria was set to 5×10^{-6} and monitored for the x- and y-velocity, for k and ω, and for the continuity equation given in Equation 3. There were also

set convergence criteria for five monitor points in the flow. The placement of the monitor points and the simulation details are listed in Table 2.

Table 2: Simulation details for the calibration case and the cases studied in this thesis.

Fluid	water
Density of fluid	$\rho = 998.2\,\text{kg m}^{-3}$
Viscosity of fluid	$\mu = 0.001\,\text{kg m}^{-1}\text{s}^{-1}$
Turbulence intensity	5%
Inlet diameter	$D = 97\,\text{mm}$
Grid element size	$h = 3\,\text{mm}$
Residual criteria	5×10^{-6}
Convergence criteria for monitor points	0.0009
Maximal iterations per time-step	5000
Monitor point coordinates	$x = 0.97 \quad y = 0.05$
	$x = 1.03 \quad y = 0.05$
	$x = 1.10 \quad y = 0.05$
	$x = 1.12 \quad y = 0.07$
	$x = 1.13 \quad y = 0.15$

3.1 Calibration

An article by Yu et al. [23] describing the coherent structure of an impinging jet was used to calibrate the transient injection of substrate in TR. As a result, the geometry was modified to have similar properties as the channel used by Yu et al. The plate was removed, and the distance between the inlet and the reactor floor was elevated to twice the inlet's diameter. To save computational power, the geometry was modified to only include the lower half of the tank. Figure 8 shows a drawing of the computational domain as well as the measurements for recreation purposes. The mesh for the calibration case was generated by using quadratic cells of cell size $h = 3\,\text{mm}$. The number of cells in the mesh was 139 866. A screen shot of the mesh from ANSYS Meshing is shown in Figure 8.

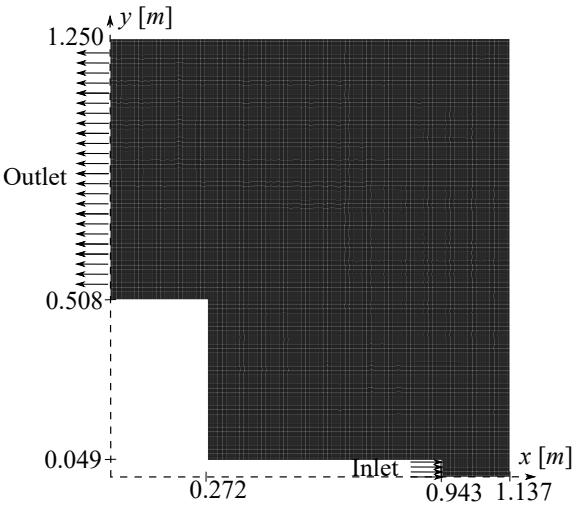

Figure 8: The computational domain of the calibration case. The drawing shows the dimensions of the domain together with the inlet and the outlet. The mesh is generated with quadratic cells and has a cell size of $h = 3\,\text{mm}$.

The velocity at the inlet and the simulation time was chosen to match the system of Yu et al. The Reynolds number was 8500, yielding an inlet velocity of $U_{max} = 0.088\,\text{ms}^{-1}$. The time scale was calculated by

$$T^* = \frac{D}{U_{max}} \tag{26}$$

giving $T^* = 1.102\,\text{s}$. Based on the development of the flow simulated by Yu et al., the end time was chosen to be $T = 120$ which equals 132 s for this flow. For the calibration case to fulfill the CFL condition from Equation 25 was therefore Δt set to 0.034 s. The convergence criteria for the residuals were first set to 5×10^{-5}, then to 1×10^{-5}, and finally to 5×10^{-6}, before the velocity magnitude for the five monitor points was plotted against time. To make the solver iterated until convergence, the number for maximum iterations per time-step was set to 5000. After plotting the resulting velocity development for the monitor points, 5×10^{-6} was decided to be sufficient and the simulation results from this simulation were therefore used as the basis for comparison with

the results from Yu et al. A summary of the simulation details for the calibration case is to be found in Table 3.

Table 3: Simulation details for the calibration case.

U_{max}	$0.088\,\mathrm{ms}^{-1}$
Δt	0.034 s
T^*	1.102 s
Simulation time	132 s
Number of time steps	3600
Number of cells	139 866
Re	8500

The results from the simulations were further collected and compared to the results from Yu et al. The vortex placement and development at the instantaneous time frames of $T = 10$, $T = 50$, $T = 100$, and $T = 120$ were compared to Yu's plot of the vorticity at the corresponding time frames. From the simulations were the streamlines and the velocity magnitude plotted to describe the flow pattern. All the plots were then used as a basis for comparison to decide and discuss whether the time development of the flow was accurate.

To address the application uncertainty of the viscosity in the problem, two simulations were run with different viscosities. The two simulations were run with $U_{max} = 0.6\,\mathrm{ms}^{-1}$ and $T = 111$. The viscosity of the first simulation was $\nu = 1.01 \times 10^{-6}$ $\mathrm{kgm}^{-1}\mathrm{s}^{-1}$ which is the default viscosity of water in ANSYS Fluent. For the next simulation, the viscosity was doubled.

3.2 Case study

The case study consisted of nine cases with the aim to deduce recommendations for optimizing the mixing of new substrate in TR. The concept of increasing dispersing of kinetic energy across the volume, as described in the literature [16], was used to determine ideal mixing settings. An overview of the nine cases is given in Table 4. The first three cases were investigated to observe the effect of changes in inlet velocity and pump duration. The case dispersing the kinetic energy throughout the domain as described desirable by literature was then chosen and used as a basis for the next six cases. Case 4-6 aimed to investigate whether the distance from the inlet to the bottom of the reactor tank changed the mixing pattern. The geometry, which distributed the kinetic energy and was considered practical in terms of empirical operational experience, was chosen for further investigation. For Case 7-9, Geometry 2 was used, and the distance from the plate to the floor was adjusted for each case. These cases were further compared to Case 1-6 to investigate whether it was possible to find some recommendations for optimizing the mixing of new substrate in TR.

Table 4: Description of the details for the cases used in the case study. The inlet velocity are given by U_{max}, while L and l is specified lengths in the reactor described by the diameter of the inlet D.

Case	U_{max} [ms^{-1}]	Simulated time [s]	Geometry	L	l
Calibration	0.088	132			
1	0.1	108		$2D$	
2	0.25	43			
3	0.6	18	1		
4	Best of Case 1-3			$3D$	
5				$4D$	
6				$5D$	
7				Best of Case 1-6	$0.5D$
8			2		D
9					$1.5D$

Case 1-3 sought to determine whether velocity or pump duration had the greatest influence on the

mixing. As described in subsection 2.2, the new substrate is heated in an active heat exchanger before being flushed into the AD tank. The pump duration was therefore calculated with the size of this heat exchanger as the limiting property. One injection of substrate was assumed to be 80 L. Therefore, adjustments were made to the simulated time to correlate this time to the inlet velocity. Because of the log-linearity between U_{max} and the pump duration time, the three velocities shown in Figure 9 were chosen. For the mesh of Case 1-3 was the calibration mesh used. The simulation details for Case 1-3 are presented in Table 5 and will be discussed in later sections. The simulation results were further plotted and described in later sections to provide recommendations for the inlet velocity.

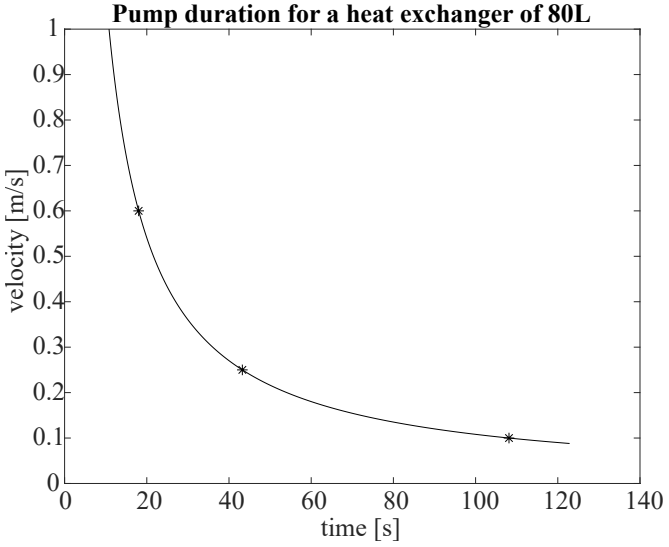

Figure 9: The pump duration time for an active heat exchanger of 80L as a function of the inlet velocity.

Table 5: Simulation details for Case 1-3.

	Case 1	**Case 2**	**Case 3**
U_{max}	$0.10\,\mathrm{ms}^{-1}$	$0.25\,\mathrm{ms}^{-1}$	$0.60\,\mathrm{ms}^{-1}$
Δt	0.030 s	0.012 s	0.005 s
T^*	1.103 s	0.388 s	0.162 s
Simulation time	108 s	43 s	18 s
Number of time steps	3600	3600	3600
Re	9658	24 144	57 946

Case 4-6 aimed to determine how the distance from the inlet to the floor affected the mixing. Therefore, one of the cases from Case 1-3 was used as the inlet boundary condition with the appropriate simulation time, time step, and Reynolds number. In addition, L was changed from 2D to 5D, where Case 4 conducted using $L = 3D$. Case 5 and Case 6 were further conducted using $L = 4D$ and $L = 5D$ respectively. For the mesh, the setup was similar to the validation case with $h = 3\,\mathrm{mm}$ and quadratic cells. The number of cells for Case 4-6 are given in Table 6. The solutions were further compared to each other and the cases from Case 1-3 for discussing recommendations for the distance to the floor.

Table 6: Number of cells in the meshes of Case 4-6.

	Number of cells
Case 4	139 413
Case 5	139 915
Case 6	140 603

Case 7-9 investigates the effects of the inserted plate. The plate was inserted into the system to protect an installation in the floor of TR. It was therefore interesting to observe how this would disturb the flow. L was kept according to the earlier simulation's recommendations, while l was adjusted. In Case 7 was the simulations conducted using $l = 0.5D$, while Case 8 and Case 9 used $l = D$ and $l = 1.5D$ respectively. The mesh for these simulations was generated as the calibration case with quadratic cells of 3 mm, and the number of cells may be found in Table 7. For the inlet boundary condition, the recommendation of Case 1-3 was used. The solutions from Case 7-9 were further compared to each other as well as the case with no plate, before recommendations for the geometry concerning mixing were discussed according to theory and operational experience.

Table 7: Number of cells in the meshes of Case 7-9.

	Number of cells
Case 7	139 413
Case 8	139 626
Case 9	139 907

3.3 Recirculation pump

A recirculation pump simulation was conducted due to large deviations between the case study results and the known steady state solution presented in section 1.1. In the case of inserting a recirculation pump into the system of TR, the pump duration will be important to discuss. To obtain an order of magnitude of which the tank is sufficiently mixed, Case 3 was run for 62400 time steps and the solution for the velocity field was extracted at every 600 time step. The velocity field was further plotted together with the flow zones described in subsection 2.1. The steady state solution in Figure 1 and Figure 2 from section 1.1 and was used to evaluate the solution at every time step. Furthermore, the importance of evaluating pump energy consumption and increasing biogas yield was discussed based on the findings.

Based on the steady state simulation, the domain was enlarged to contain the whole liquid phase of the reactor. The bottom 1.137 m had the same geometry as described in the calibration case and shown in Figure 8. The outlet was then extended 1.43 m in the negative x-direction without changing the bottom part of the domain. The mesh was generated with quadratic cells of $h =$ 3 mm and the number of cells in the resulting mesh was 258,417. Figure 10 shows the mesh of the domain together with the dimensions of the domain.

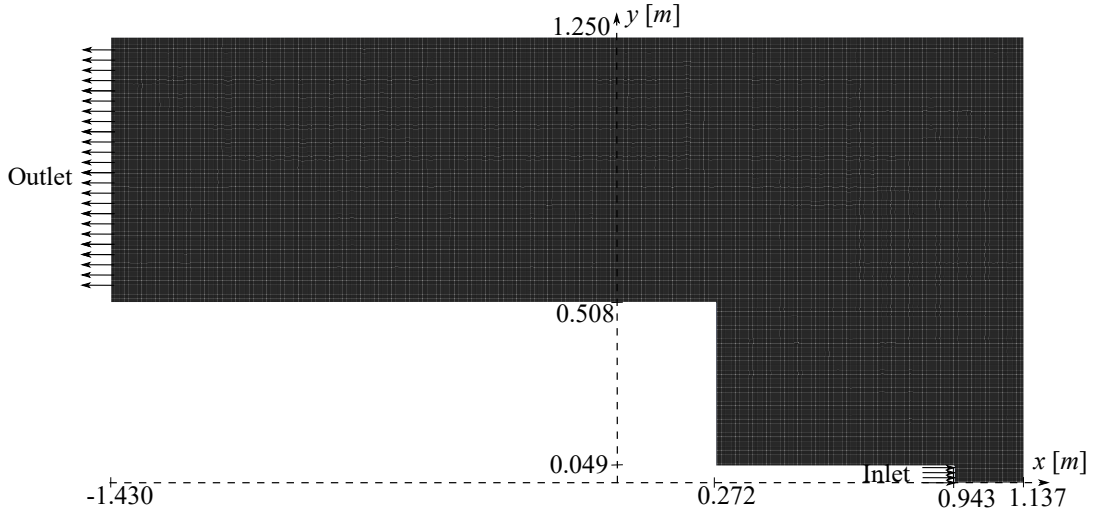

Figure 10: The mesh of the entire domain with a 3 mm grid and the domain's dimensions.

3.4 Particle injections

To understand how particles can be expected to be transported through the domain, particle injections were simulated. The domain and setup for the fluid phase of the particle simulations were taken from the recirculation pump and Case 3 respectively. The mesh used was the mesh of the recirculation pump in Figure 10. Furthermore, the simulation details from Table 5 for Case 3 and Table 2 were used for the continuous fluid phase. A particle phase was further set up by introducing an inert particle of the density $\rho_p = 1070\,\mathrm{kg\ m^{-3}}$ to the list of materials. To simulate the settling nature of the particles, gravitation was set to $9.81\,\mathrm{ms^{-2}}$ in the x-direction. Because it was of interest to investigate how the new substrate was distributed in the tank, the granules were inserted through the inlet with a stream velocity of $0.6\,\mathrm{ms^{-1}}$. The duration was set to 18 s which corresponds $T = 111$, and the total flow rate was calculated to $0.178\,\mathrm{kg\ s^{-1}}$, based on 4% TS. The size distribution and particle density were based on an article from USN written by Tassew et al. [15]. A Rosin-Rammler distribution with the parameters shown in Table 8 was found to estimate the size distribution of the study by Tassew et al. [15], and was therefore used to model the particle size distribution. The number of diameters in the simulation was further set to 10, and Fluent's standard parcel release method was used to insert the particles into the domain. The particles were further simplified to spherical particles, and the discrete random walk model was not enabled. For physical models, the virtual mass force and the pressure gradient effects was enabled due to the ratio of the densities in the flow being greater than 0.1. Discrete element method (DEM) collisions were discussed but decided to be out of scope together with the gas-phase modelling.

Table 8: Parameters for the Rosin-Rammler distribution of particles from 4% TS pig manure.

Min. diameter	0.100 mm
Max. diameter	1.60 mm
Mean diameter	0.704 mm
Spread parameter	3.4

The need for two-way coupling was further investigated by simulating until $T = 45$ with both one- and two-way coupling. This method was chosen due to lack of available information to calculate the Stokes number of the particles. For the one-way coupling, interaction with the continuous phase was disabled in Fluent. While for the two-way coupling, this interaction was enabled and the discrete phase model update interval was set to 10. This means that the continuous phase was iterated for 10 iterations before the iterations for the discrete phase were conducted. This iteration process was then continued until a converged solution was found for the given time-step. Both simulations were run with 500 as the max number of steps for the discrete phase and a specified length scale of $h = 3\,\mathrm{mm}$. No physical models were used, and the hybrid method was chosen for the parallel. For the numerics, the tolerance was set to 5×10^{-6} with a maximum refinement factor of 20. For the tracking schemes, the automated choice was enabled and Runge-Kutta was chosen for the high order scheme, while the implicit Euler method was chosen for the low order scheme. No node-based averaging was enabled, nor was the linearization of the source terms. Because the particles in the two-way coupled simulations affect the surrounding fluid, it is of importance to control the right number of particles in the domain. Therefore, in the granule injection, the parcel release method was chosen to be a constant number of one particle per parcel. To compare the two cases, both the one- and two-way coupled simulations were run with this parcel release method. A summary of the setup for the one- and two-way coupled simulations is to be found in Table 9. Finally, the simulation results were post processed and compared in order to investigate whether a two-way coupled simulation was necessary.

Table 9: Summary of the simulation setup details for the one- and two-way coupled simulations.

	One-way coupled	**Two-way coupled**
Simulation time	$T = 45$	$T = 45$
Interaction with continuous phase	disabled	enabled
Discrete phase model interval update	-	10
Max. number of steps	500	500
Specified length scale	3 mm	3 mm
Physical models	Virtual mass force Pressure gradient effects	Virtual mass force Pressure gradient effects
Parallel method	Hybrid	Hybrid
Tolerance	5×10^{-6}	5×10^{-6}
Max. refinement factor	20	20
High order scheme	Runge-Kutta	Runge-Kutta
Low order scheme	Implicit Euler	Implicit Euler
Node based averaging	disabled	disabled
Linearization of source terms	disabled	disabled
Parcel release method	constant number = 1	constant number = 1

Furthermore, one-way coupled simulations were used to simulate particle injection in Case 3 and Case 1 with the simulation details described above. The two cases were used as inlet boundary conditions for investigating how the velocity affects the particle distribution. Case 3 with injection of particles was used as a basis for comparison for the particle simulations, similarly to the case without particle injection. Case 1 was run as an inlet boundary condition with $U_{max} = 0.1\,\mathrm{ms}^{-1}$, and the results were compared to the Case 3 particle simulations to confirm the ostensibly beneficial idea of higher velocities for new substrate mixing.

The setup for the one-way coupled simulations were further used for a simulation where the density of the particles was investigated. The aim of these calculations was to investigate how particles with a density lower than the continuous phase would advance through the domain. This was intriguing since the granules' density naturally fluctuates dependent on their internal gas generation. A second phase of particles was therefore added to the simulations. The density of these granules was chosen to be $\rho_p = 926.4\,\mathrm{kg\ m}^{-3}$. Because there was no model for particle-particle interaction and the simulation was one-way coupled, the parcel release method was set to standard for less computational demand. The rest of the discrete phase model parameters were kept as described above.

Due to the introduced recirculation pump, a simulation with particle injection in a recirculation pump flow was conducted. This was simulated by using the one-way coupled set up with the standard parcel release method and the particles with $\rho_p = 1070\,\mathrm{kg\ m}^{-3}$. The simulation was run until $T = 1500$ based on the simulations for the recirculation pump without particle injection. Through the simulations, the results were exported every 12000 timestep, which in real flow time translates to every minute. The particle injection was only injecting the first 18 s to simulate the injection and distribution of new substrate in the tank. After 18 s were the particle injection stopped and the inlet boundary condition was then only containing the continuous fluid phase of velocity $U_{max} = 0.6\,\mathrm{ms}^{-1}$. The results were then post processed and the particle distribution of the different snapshots was compared to both each other and the case with no recirculation pump.

4 Results

This section aims to present the results from the simulations described above. First, the calibration results will be presented and compared to literature for the purpose of assuring a physical transient development of the flow. Secondly, the results of the case study will be presented before the recirculation pump results are plotted and described. These results aim to point out differences and similarities between the simulations for the purpose of finding general recommendations for TR. Lastly, the particle injection results will be presented, which aim to both describe the weaknesses

and strengths of the model, as well as present the results for different flow situations. The particle simulations will therefore be used as a foundation for predicting how the biogas yield is affected by different configurations, which will be discussed in section 5.

4.1 Calibration

The calibration resulted in the flow shown in Figure 11 where a vortex is developing next to the inlet. This figure presents plots of the velocity magnitude and the streamlines for the flow in four different non-dimensional points in time. Similar to all the plots, is the vortex forming on the outside of the jet. However, the placement of this vortex depends on the time of development. For $T = 10$, the vortex center is placed approximately at $x = 0.92\,\text{m}$ $y = 0.20\,\text{m}$ and is therefore located above the inlet of the jet. Furthermore, the jet is forcing the velocities along the reactor's floor to increase, despite the fact that the velocity magnitude in this location is low at this instant. For the next snapshot, at $T = 50$, the high velocity has reached the floor of the reactor, causing the vortex to move both downwards and sideways in the volume. The location of the vortex center in this instant is approximately $x = 1.06\,\text{m}$ $y = 0.24\,\text{m}$. The trend is further developing for $T = 100$ where the velocity along the floor is further increased and the vortex center has moved to approximately $x = 1.02\,\text{m}$ $y = 0.41\,\text{m}$. The vortex center is approximately located at $x = 1.01\,\text{m}$ $y = 0.46\,\text{m}$ for the final time step, $T = 120$, demonstrating the trend of pushing the vortex radially through the tank. Consequently, a vortex generation can be seen in the calibration as first traveling axially towards the floor before changing direction and travelling along the floor in the radial direction.

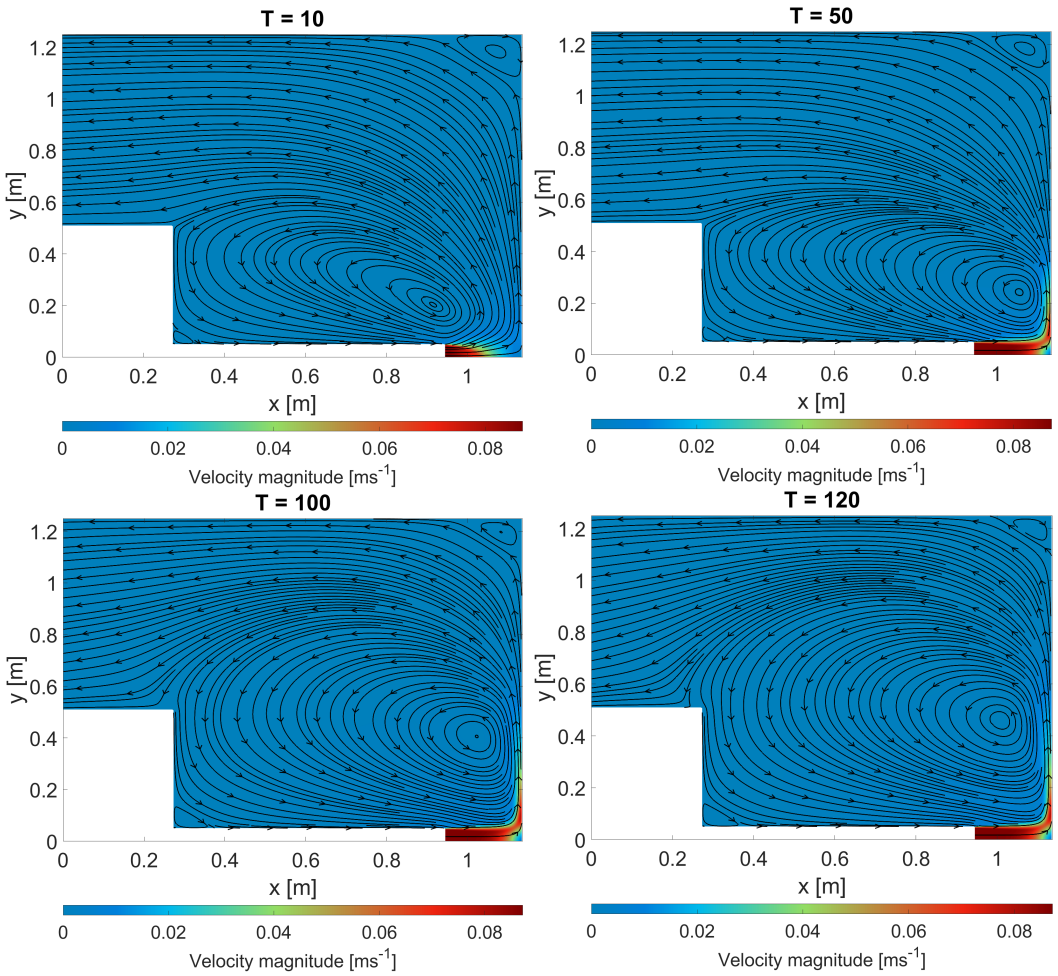

Figure 11: Plot of the velocity magnitude and the streamlines for snapshots of the calibration. T denotes the dimensionless time of the system.

When comparing these results with the results from Yu et al. [23] shown in Figure 12, some of the same trends occur. The vortex is spread towards the outlet of the system, and the center moves from close to the inlet towards the floor before moving along the floor. However, in this case, the flow is bounded by an upper and lower plate, limiting vortex formation between the two plates. In other words, the center of the vortex will always be placed below the inlet of the jet. This is in contrast to the vortex formation described in the results from the calibration above. It is also to be noted that the representation of the results from Yu et al. [23] are different compared to the representation chosen for the calibration. Yu et al. have chosen to plot the vorticity of the flow, while the calibration results present the streamlines and velocity magnitude of the flow. Both representations do, on the other hand, aim to visualize the vortex development, which is similar despite the difference in geometry.

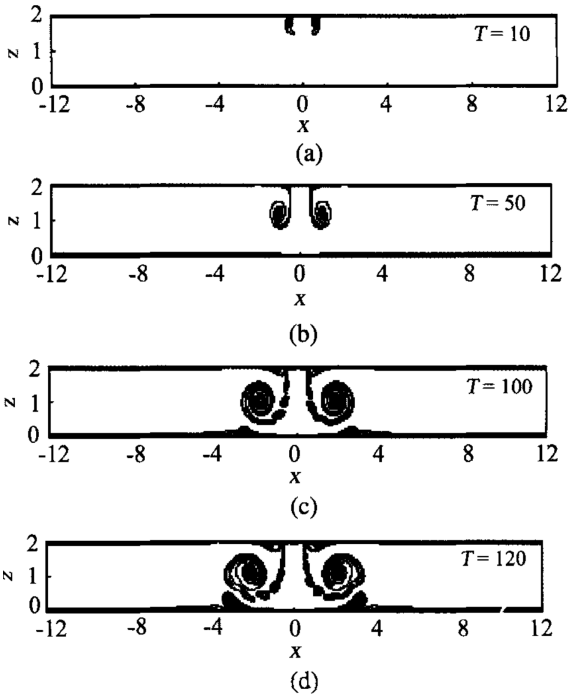

Figure 12: Vorticity plot from Yu et al. showing the vortex development as a function of time in-between two plates.

Source: [23]

Simulation with three different residual criteria revealed the system to vary with the size of this stopping criteria. The velocity in the monitor points was used as an indicator and a plot of the velocity development for different residuals is shown in Figure 13. The plots show that the velocity development varied with the residual criteria chosen for the problem. A residual criteria of 5×10^{-5} shows a solution with large deviations compared to the smaller criteria. The criteria of 1×10^{-5} and 5×10^{-6} shows velocity developments of the same character for all of the monitor points chosen. Based on these plots, residual criteria of 5×10^{-6} were chosen to be sufficient for convergence within each timestep.

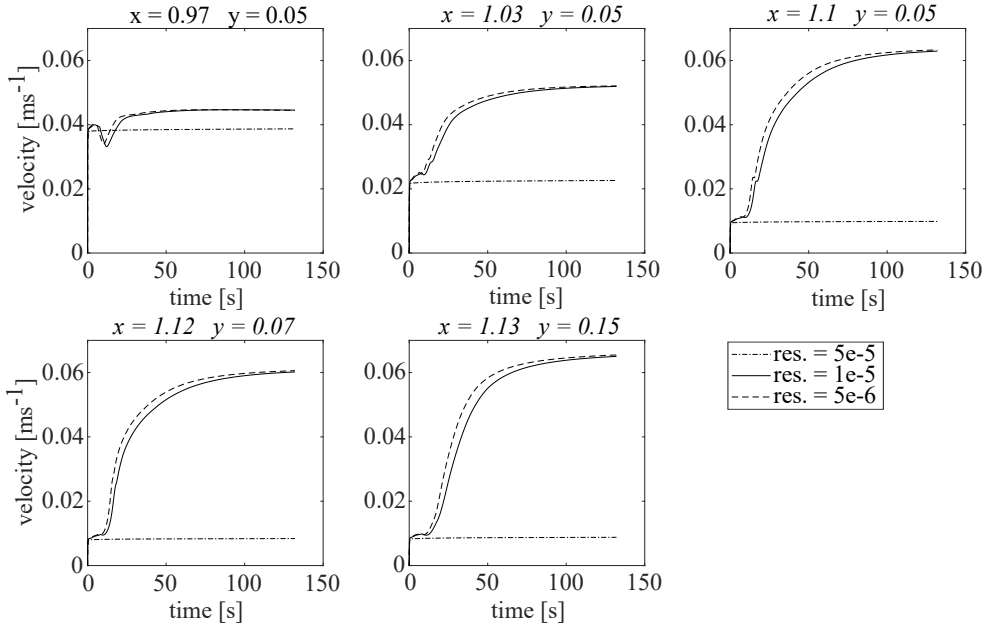

Figure 13: Plot of the velocities at the five monitor points of the flow for three different residual criteria. Above the plots are the coordinates of the monitor points given in meters.

When the viscosity of the fluid inside TR was doubled, the flow changed marginally, which can be observed by Figure 14. The corner vortex, where the floor of the reactor meets the wall, is greater in the plot of doubled viscosity than in the case when the viscosity is equal to the viscosity of water. It may also be noted that the emerging jet vortex is somewhat closer to the jet centerline. Nonetheless, the differences between the flow field and the remainder of the flow field are minimal. It is also difficult to distinguish the variations in velocity magnitude between the two scenarios. As a result, the viscosity is projected to have only a modest impact on the flow development in TR.

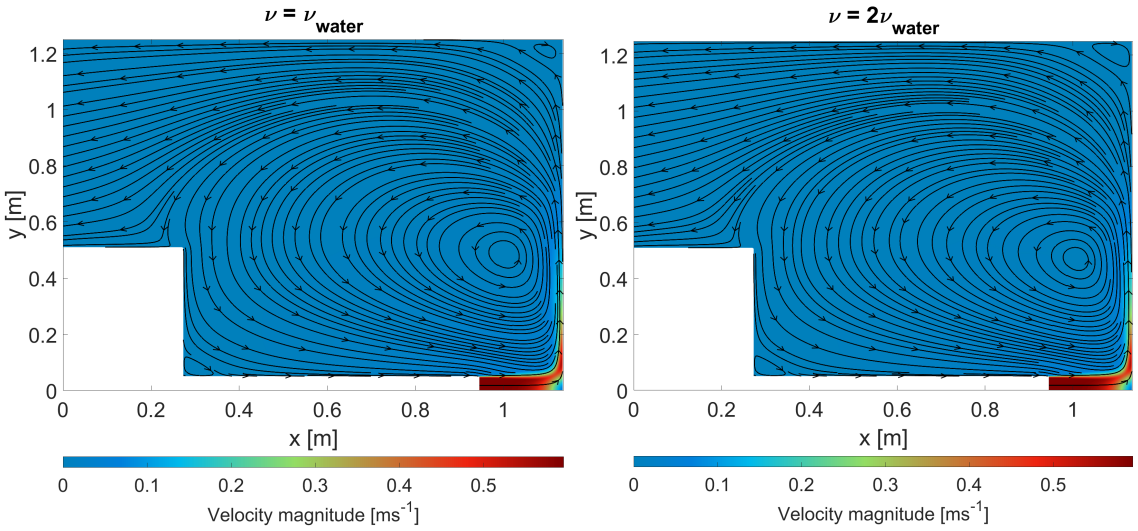

Figure 14: Plot of the velocity magnitude and the streamlines for different values of the viscosity. T denotes the dimensionless time of the system and ν_{water} represents the viscosity of water.

4.2 Case study

Case 1-3 revealed that the flow patterns of the three cases were almost identical, with just the amplitude of the velocities in the tank changing. The purpose of these three scenarios was to study the effects of modifying the inlet velocity and pump duration. Case 1-3 was run for $T = 111$, demonstrating that the time horizon for the three examples is equivalent. This may also be observed when addressing the simulations presented in Figure 15. Figure 15 shows the velocity magnitude and the streamlines for the three cases at $T = 111$. The streamline plots for Case 1-3 are nearly identical, indicating that the flow has achieved the same phase of development. The flow pattern deduces the indication from the non-dimensional time scale, demonstrating comparable flow development for the three cases. The velocity magnitude plots change because the three scenarios were conducted with variable inlet velocity, U_{max}. Case 3 spreads a greater quantity of kinetic energy throughout the domain due to its high velocity. This is visible in the velocity magnitude contour plots, where the stream evolution is almost identical but the velocity in Case 3 is greater. In other words, when Case 3 is applied, there is more kinetic energy dispersed than when Case 1 or Case 2 is applied. Case 3 was thus chosen as the inlet boundary condition for the remaining simulations.

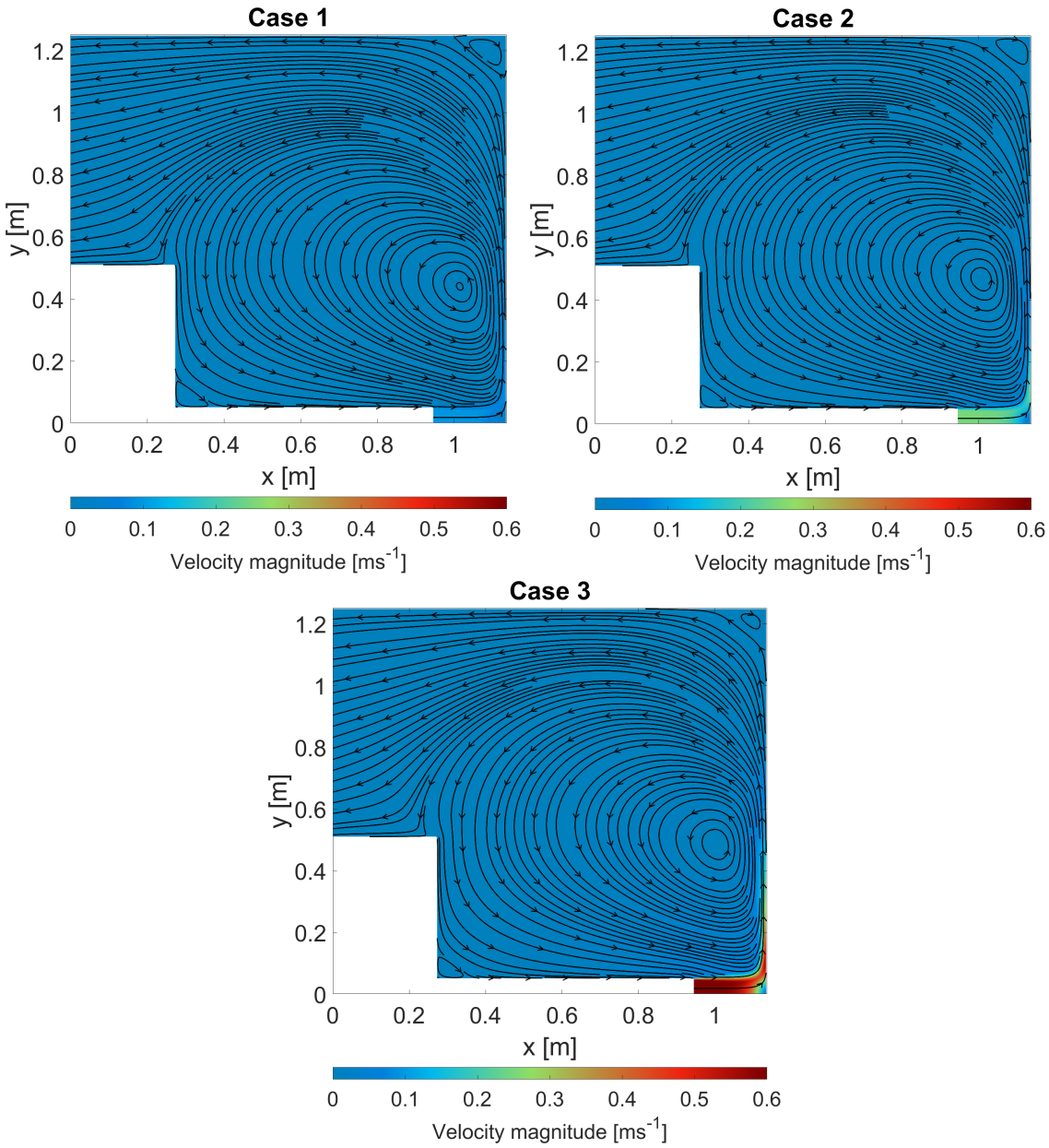

Figure 15: Plot of the velocity magnitude and the streamlines of Case 1-3.

When studying the mixing impact, simulation of Case 4-6 revealed that the distance from the inlet to the reactor floor was of modest interest. The distance L in Case 4-6 was adjusted from $2D$ in Case 3 to $5D$ in Case 6 to study the effect this length had on the mixing. Case 3-6 are plotted in Figure 16, demonstrating reduced variations in kinetic energy spreading when analyzing Figure 16 versus analyzing Figure 15. This suggests that the velocity and pump duration have a greater influence on mixing than the distance from the inlet to the floor. However, the streamlines suggest that the center of the vortex moves closer to the inlet as L increase. That is, the vortex has swirled less of the region along the tank's bottom surface. The vortex, on the other hand, has traversed a larger region in the axial direction. Given the operational experience with flushing against the floor being the preferred option for mixing, $L = 2D$ from Case 3 was chosen to be the preferred L for the remaining simulations.

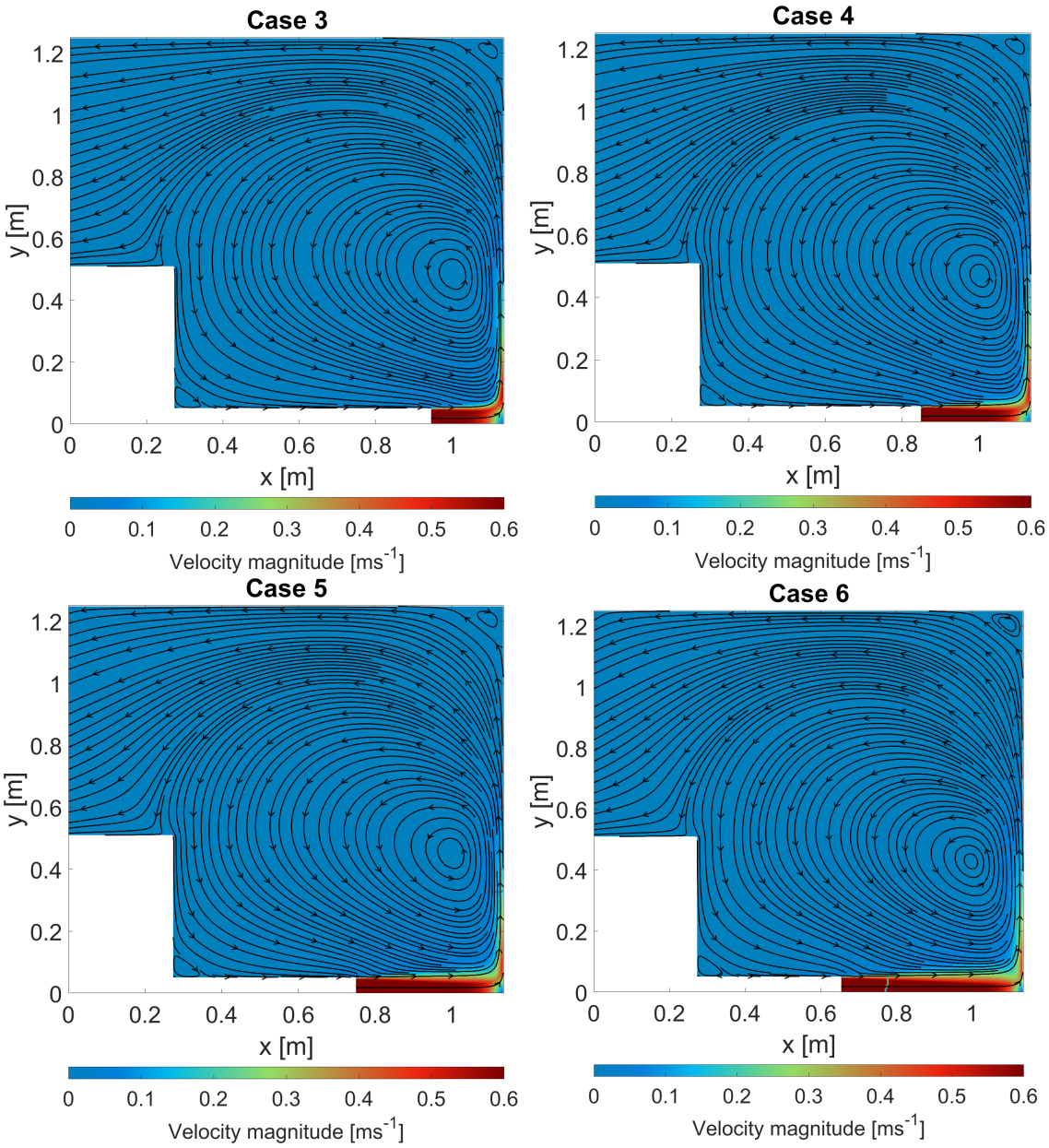

Figure 16: Plot of the velocity magnitude and the streamlines of Case 3-6.

The results of Case 7-9, as shown in Figure 17, expose the plate as an unwanted complication to the geometry when enhancing of new substrate mixing is studied. The plots depict the effect of the raised plate as the distance between the plate and the floor, l, is adjusted. According to this figure, the plate's influence on the primary velocity field and vortex generation is modest. Figure 17 do, however, show a vortex formation underneath the plate. This vortex increases slightly as the length of l increases, but it seems to have a diminishing velocity magnitude. Because the overall distance to the floor is increasing in these cases, the velocity magnitude near to the floor is decreasing for increasing l values. As a result, the plate appears as an unwanted complication to the geometry. Case 3 was chosen as the preferred case of the cases studied, although in the case of placing a stagnation plate in TR, a minimal value for l appears to be preferable.

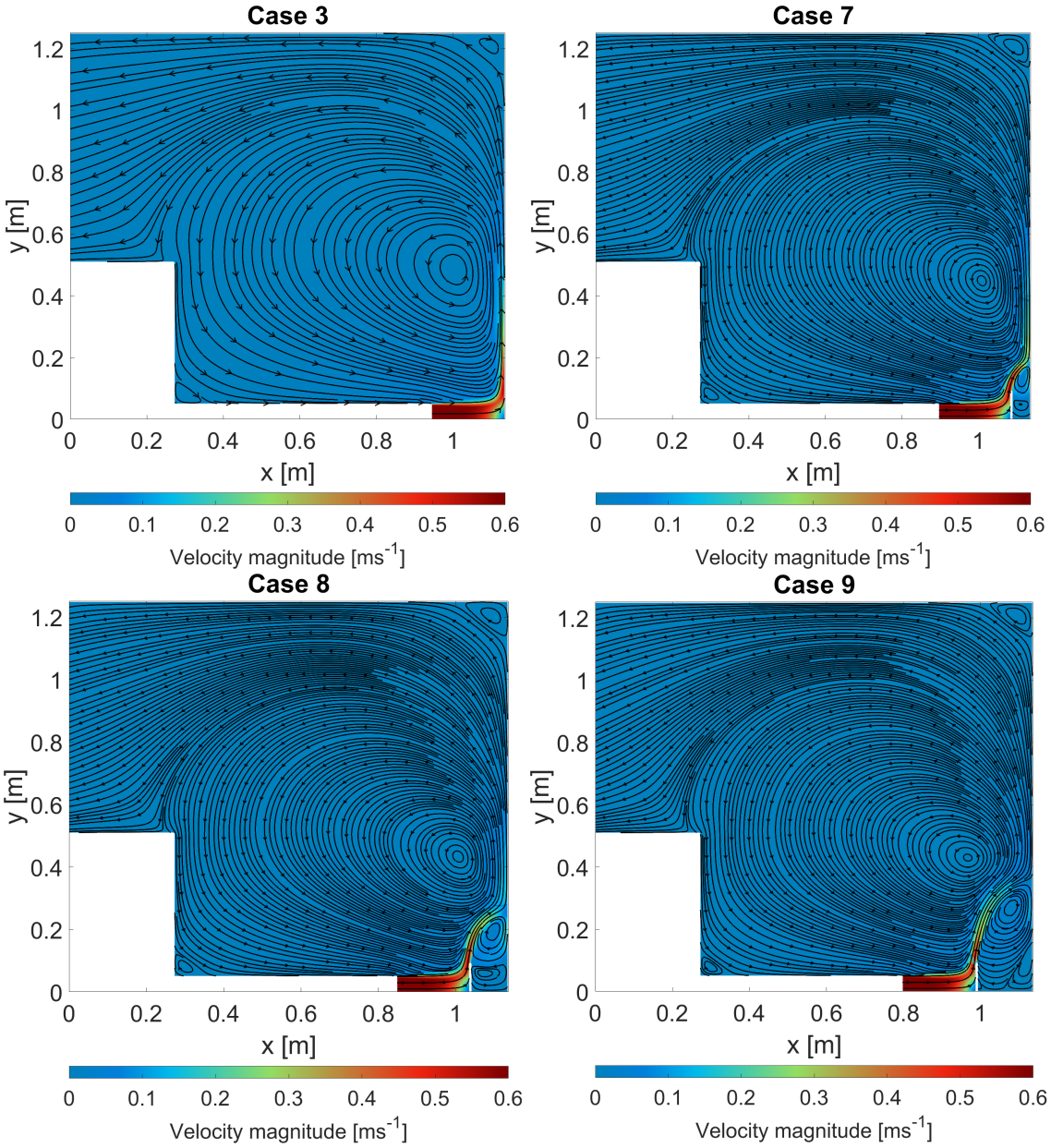

Figure 17: Plot of the velocity magnitude and the streamlines of Case 3 and Case 7-9.

4.3 Recirculation pump

The recirculation pump simulations revealed an increased spread of kinetic energy when increasing the pumping time. This section aims to describe the snapshots taken at five increased times of the flow for the purpose of explaining the increased spread of kinetic energy. Figure 2 in section 1.1 presents the flow zones of TR in the case of steady state flow appearing. i.e., increase of pump duration after reaching this state will not be improving mixing. The flow zones of the snapshots were therefore compared to both each other and to the steady state solution, before $T = 1500$ was found to give a sufficient spread of kinetic energy. The following paragraphs will present the details of the results collected from the recirculation pump simulations.

At $T = 370$, Figure 18 depicts the flow field and flow zones of TR, with the vast majority of the tank's capacity being a poorly mixed zone. The flow field reveals a vortex location close to the wall and an increased velocity magnitude along the floor when compared to the $T = 111$ snapshot. The flow zones further show a high velocity region forming along the floor and corner of the tank.

There are further large poorly mixed zones and dead zones throughout the rest of the volume. Compared to the steady state solution from Figure 2 in section 1.1, the flow field is considered to be far from fully developed and there is reason to believe a greater mixing potential will be achieved by increasing the pump duration further.

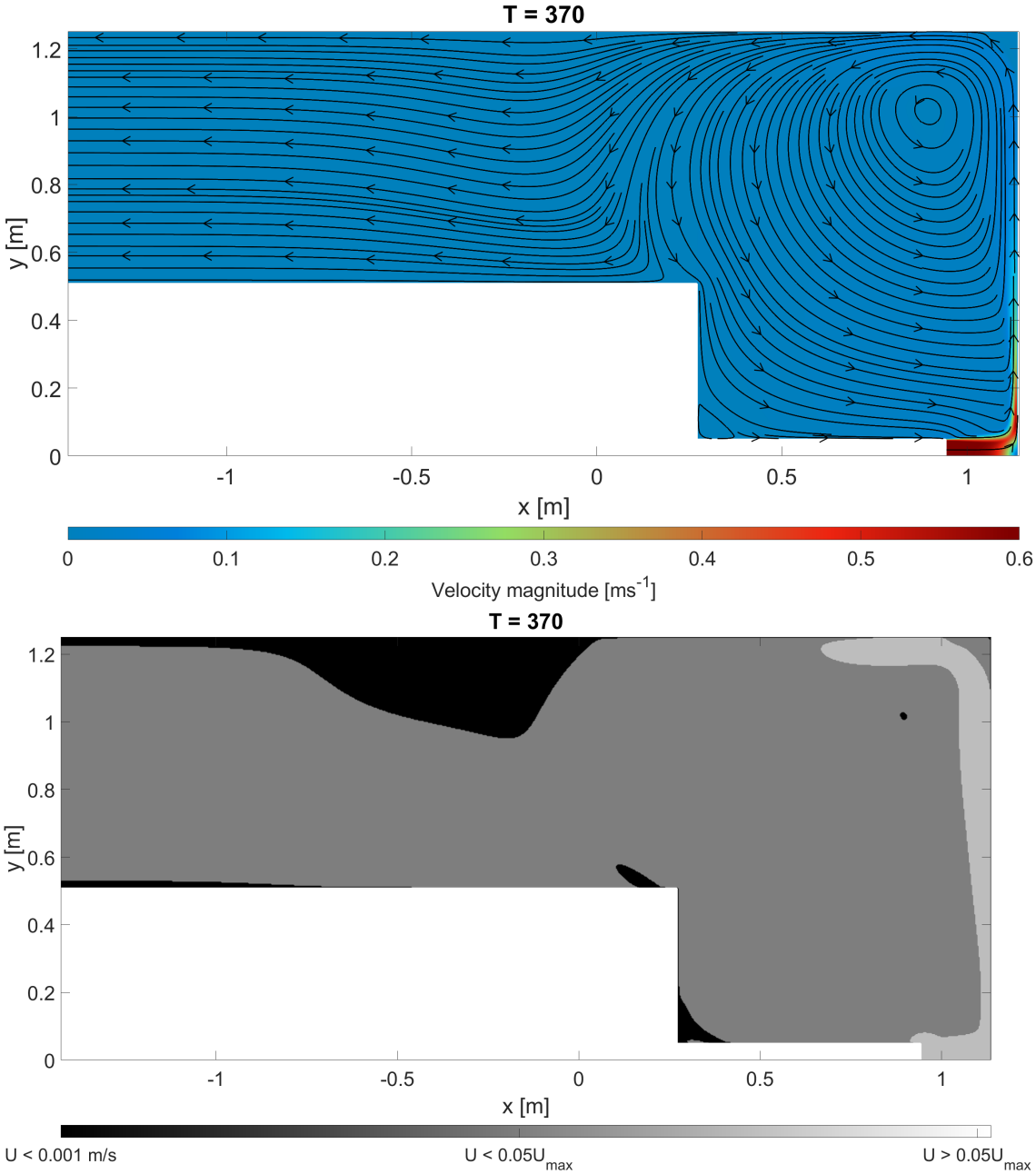

Figure 18: Snapshot of the velocity field and the flow zones of TR at $T = 370$.

Figure 19 presents the results of TR after $T = 740$, which indicates broader areas of high velocity but still reveals the tank to be dominated by poorly mixed zones. Compared to the vortex placement of the $T = 370$ snapshot in Figure 18, the vortex has, at this instant, moved both upwards and towards the center of the domain. Furthermore, Figure 19 depicts a minor vortex developing near the wall on top of the main vortex, as well as an enhanced velocity magnitude close to the wall, which expands the high velocity zone. There is however, despite the decreased dead zone volume, still a significant part of the volume considered to be a poorly mixed zone. Therefore, this solution is still far from the steady state solution.

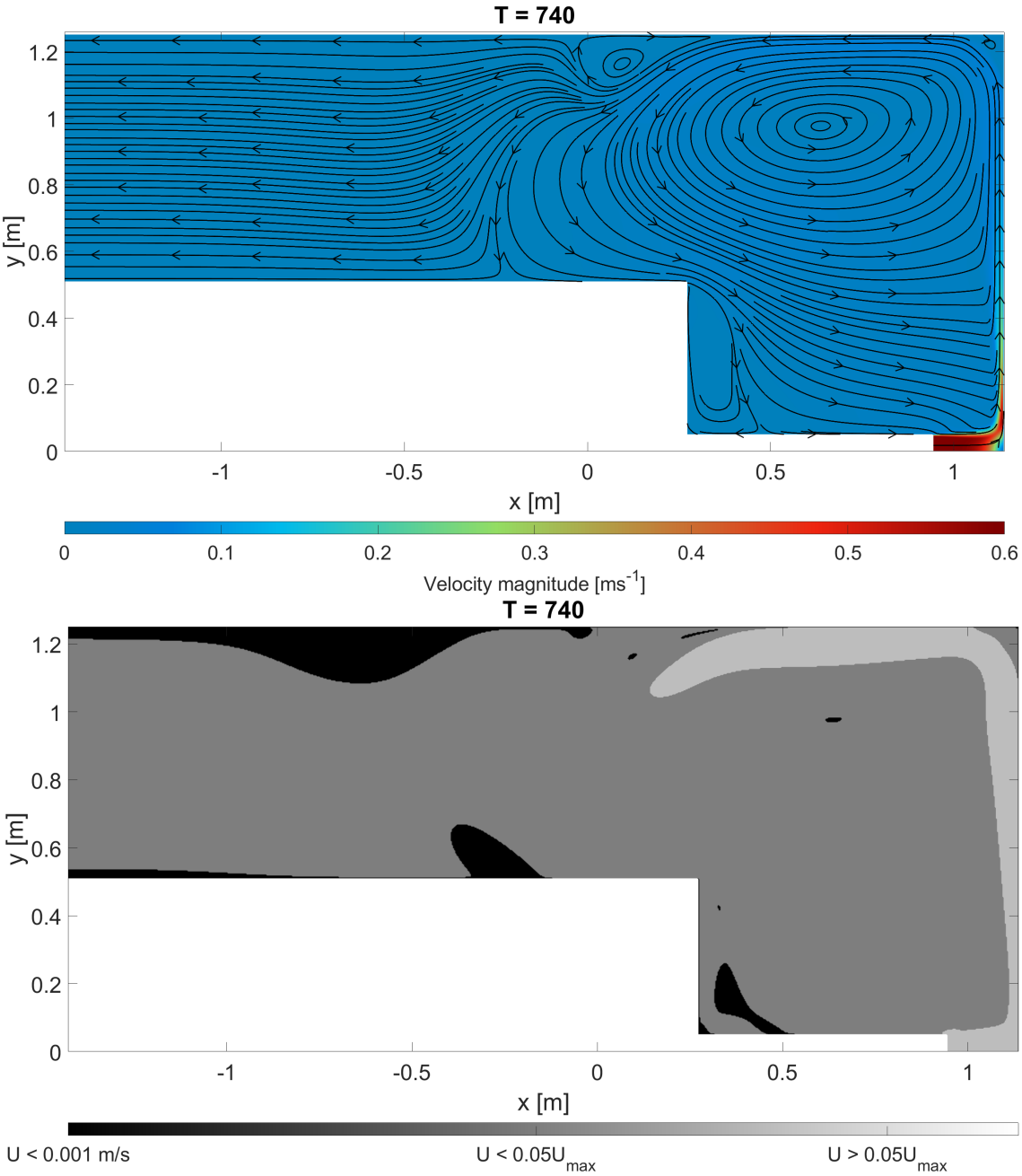

Figure 19: Snapshot of the velocity field and the flow zones of TR at $T = 740$.

The velocity field and flow zones at $T = 1100$ are presented in Figure 20 and show the lower third of the tank to be dominated by high velocity zones. From the velocity field plot, one may observe three large vortex formations. The velocity magnitude has increased in the bottom third of the tank and causes the vortex to have a high velocity region at the periphery. The small vortex forming on top of the main vortex is enlarged compared to earlier snapshots. The last vortex in the tank is placed underneath the inner tank and creates a recirculation zone between the inlet pipe and the main vortex. The flow zone plot shows an increase in volume dominated by velocities larger than 5% of U_{max}. However, there are still large areas of low velocities in the rest of the domain and it is to be expected that further increases in pump duration will decrease the size of these areas.

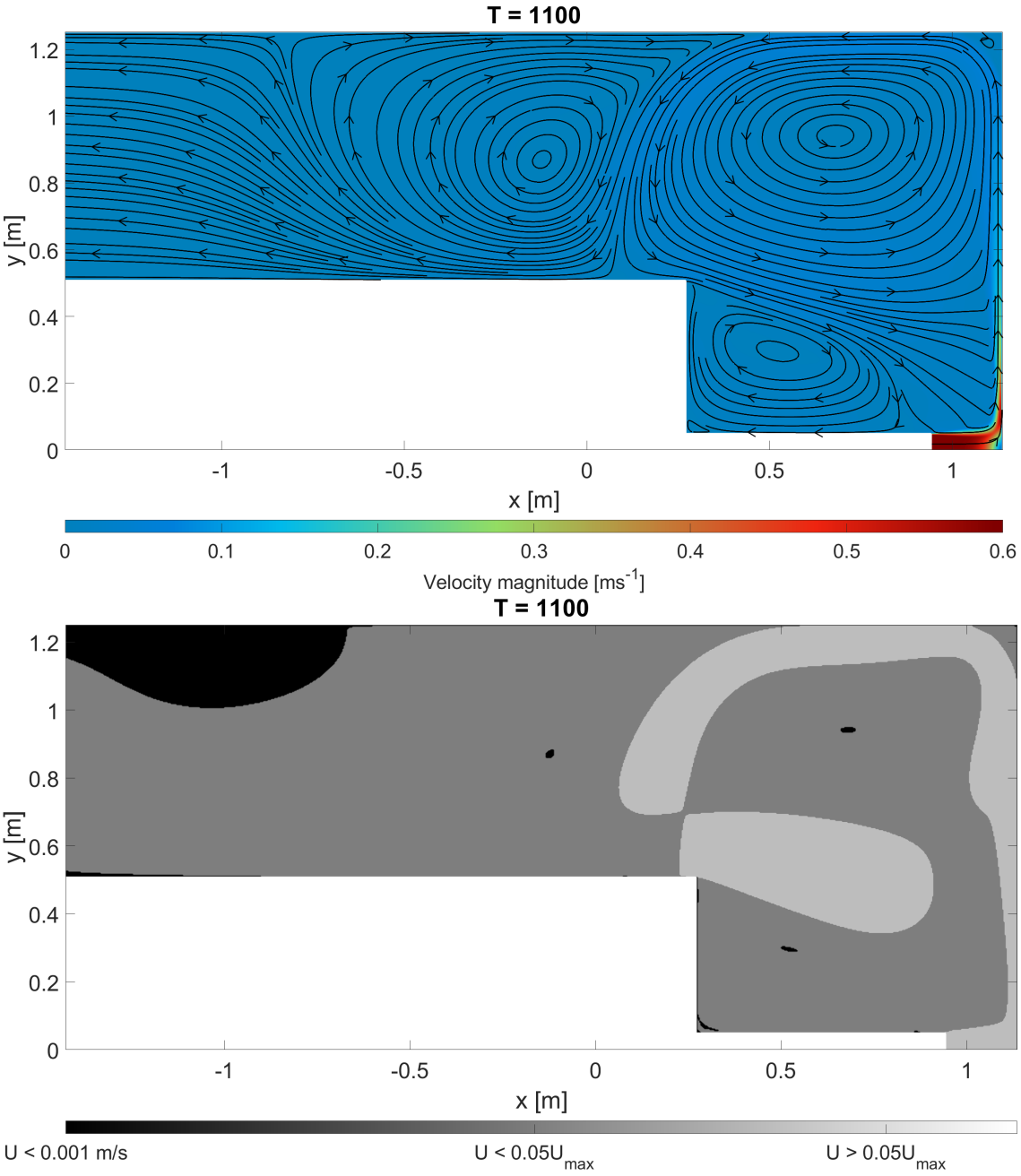

Figure 20: Snapshot of the velocity field and the flow zones of TR at $T = 1100$.

Figure 21 presents the results of the velocity field and flow zones for $T = 1500$ showing a flow pattern and flow zones similar to Figure 1 and Figure 2 from section 1.1. The main vortex has now formed a round shape, and the velocity at the periphery of the vortex has increased further. The center of the vortex on top of the main vortex has now moved towards the outlet, and the vortex under the inner tank has decreased in size. The flow zone plot reviles a high velocity zone forming along the wall of the inner tank, and one may observe the same trends as found in the steady state simulations.

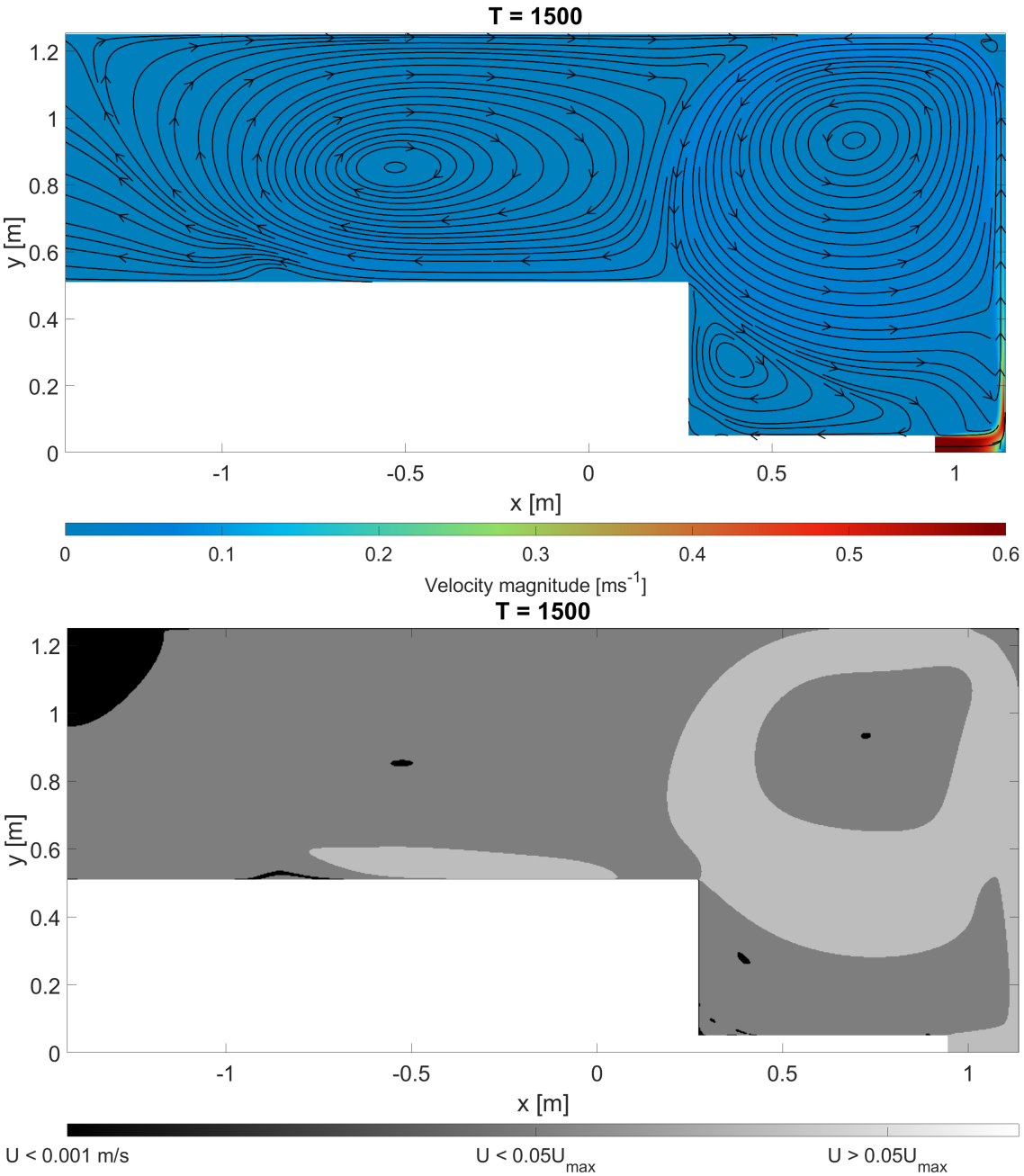

Figure 21: Snapshot of the velocity field and the flow zones of TR at $T = 1500$.

Figure 22 reveal minor changes compared to the snapshot from $T = 1500$ in Figure 21. The main vortex and the vortex under the inner tank haven't evolved considerably since the last snapshot at $T = 1500$. However, when compared to previous snapshots, the vortex on top of the main vortex has traveled farther up the tank and towards the outlet, while the dead zone volume has decreased for $T = 1900$. It should also be noted that the high velocity region has become somewhat larger. On the other hand, the increase in high velocity zones is less than earlier observed, and the gain in expected mixing effect is therefore considered to be minor.

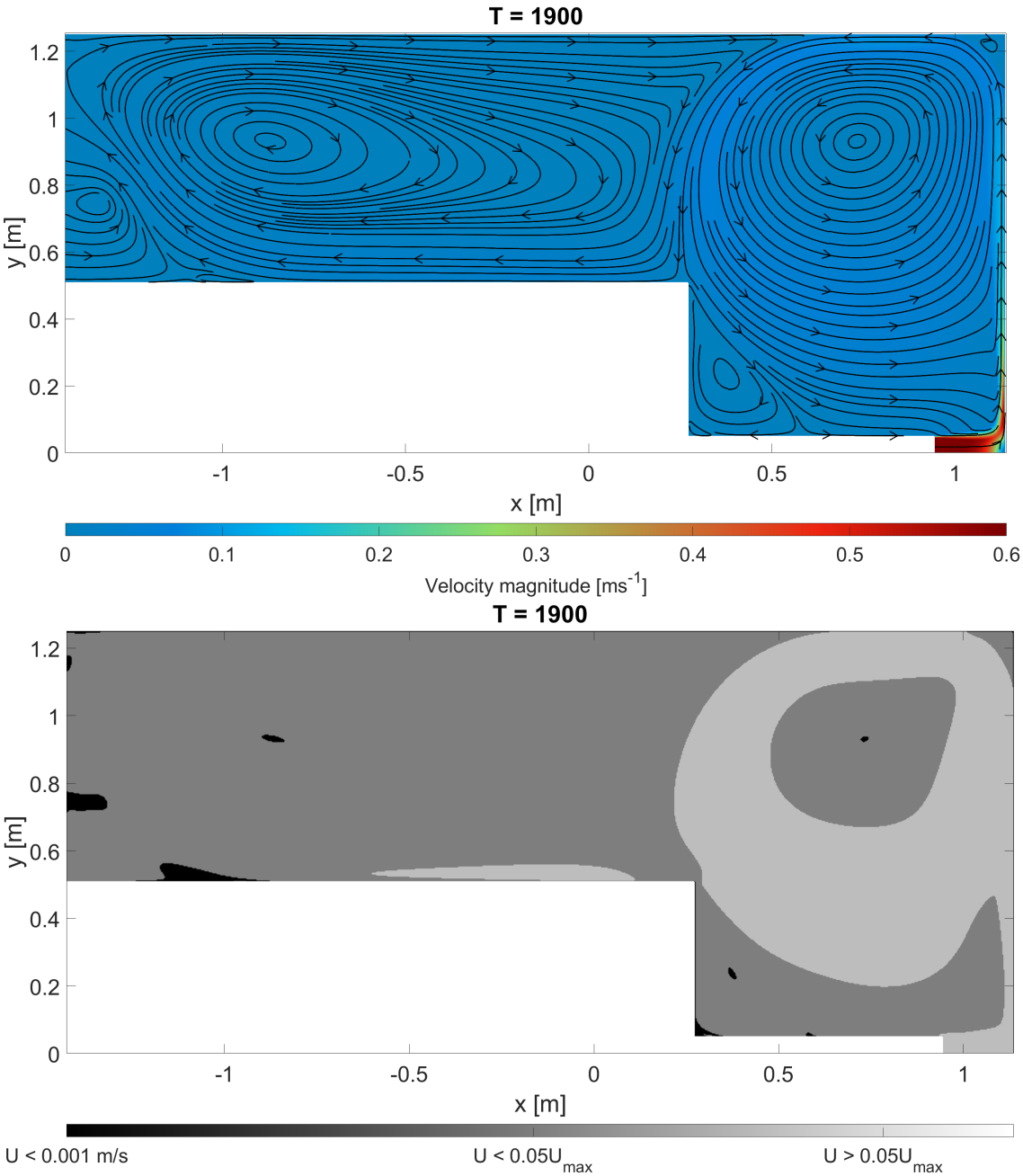

Figure 22: Snapshot of the velocity field and the flow zones of TR at $T = 1900$.

After the snapshots from the simulations had been discussed and compared side by side, and the steady state simulation, $T = 1500$ was chosen to be the appropriate pump duration for recirculation. In Figure 23, a range of inlet velocities, U_{max}, are plotted against the resulting recirculation pump duration time, t, to demonstrate the amount of time this represents duration in minutes. The plot shows that the duration is inversely proportional to the inlet velocity. As a result, low velocities result in long pump duration, whereas high velocities result in short pump duration.

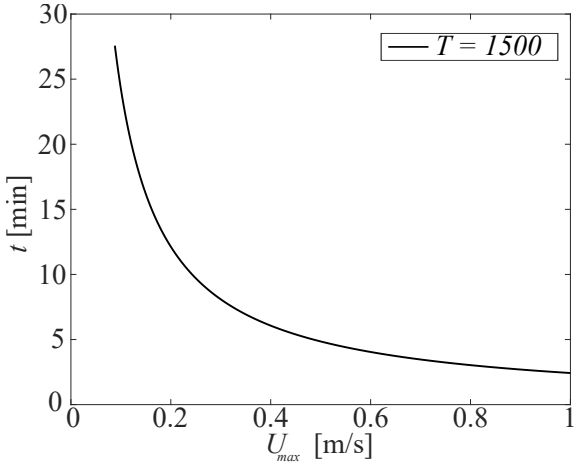

Figure 23: Plot of the recirculation pump duration time, t, and the corresponding inlet velocity, U_{max}, for the dimensionless time $T = 1500$.

4.4 Particle injections

The particle injection simulations revealed and confirmed some trends supposed throughout the simulations conducted earlier in this thesis. It was discovered that the mixing effect without the use of a recirculation pump is small, and that the volume of which contains particles, increases significantly with the introduced recirculation pump. Inlet velocity was discovered to be an important factor for mixing and the particle density was discovered to highly affect the particle path. In this subsection, the results of the particle injection simulations are presented. First, the simulations concerning one-way or two-way coupling will be addressed before the particles are injected into the volume of Case 3. Furthermore, the density of the particles, and the inlet velocity simulations, will be presented to address how these parameters affect the solution. Lastly, the recirculation pump simulation results will be presented and described to give a foundation for discussing the need for such a pump.

A one-way and a two-way coupled simulation were conducted to investigate whether it was necessary to conduct two-way coupled simulations. The results from these simulations are shown in Figure 24 and Figure 25. The right side of Figure 24 shows the resulting particle streams in the flow fields. The gray-colored particles are the particle streams from the two-way coupled simulation, while the black particles are plotted based on the results from the one-way coupled simulation. Overlapping particle streams is to be observed, except for the periphery of the swirling area. The particle streams are for both simulations swirled up from the floor by the vortex. The left part of Figure 24 presents the streamlines for the two-way coupled simulation shown in white and the streamlines for the one-way coupled simulation shown in black lines. From this plot, one may recognize a similar development of streamlines as earlier presented. Because the particles have no effect on the surrounding stream due to the one-way coupling, the plot of the black lines is identical to the streamline plot from Figure 15. The white lines, which represent the streamlines for the two-way coupling are, however, affected by the particle movements and will therefore slightly differ from the streamlines of the one-way coupled simulation. The difference appears to be notable where the vortices appear, i.e., in the corner of the tank and for the main vortex. To investigate the effect of this difference, six velocity profiles at different places in the tank were plotted for both simulations.

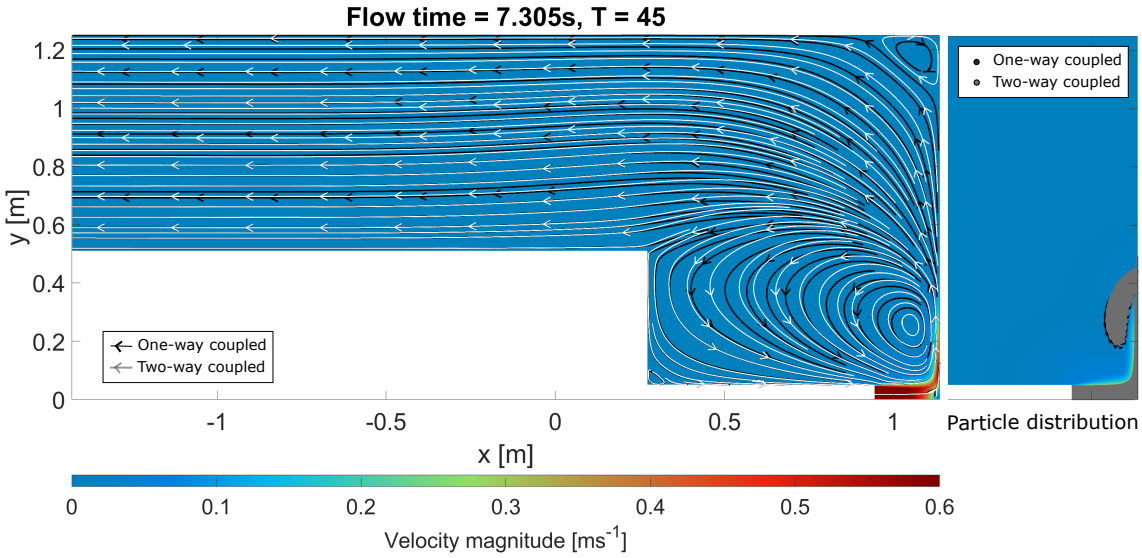

Figure 24: To the left is the simulation results from the one- and two-way coupling simulation presented. The white lines is the results of the two-way coupled simulation and the black lines is the results of the one-way coupled simulation. To the right is the bottom of the tank showing the particle distribution for one-way coupled (black dots) and two-way coupled (gray dots) shown.

The velocity profiles through points in the domain are shown in Figure 25, and it illustrates the minor influence the choice of two-way coupling has when considering the velocity magnitude. The left side of the figure displays lines travelling through different locations on the x-axis, and the right side shows velocity profiles passing points on the y-axis. Both lines are visible in the plot revealing a notable difference in the flow field. The velocity-axis is scaled to visualize the velocity in the regions of low velocity magnitudes. This does, however, cause small changes to be more visible in the low velocity plots than in the high velocity plots. On the other hand, it is important to remember the relation between force on the particle and the velocity of the flow, meaning the change in force on the particle is relative to the change in velocity. Hence, the deviations in the low velocity plots are expected to result in minor changes in the force acting on the particles. Provided these plots together with Figure 24 one may observe a difference in the flow development when conducting two-way coupled simulations.

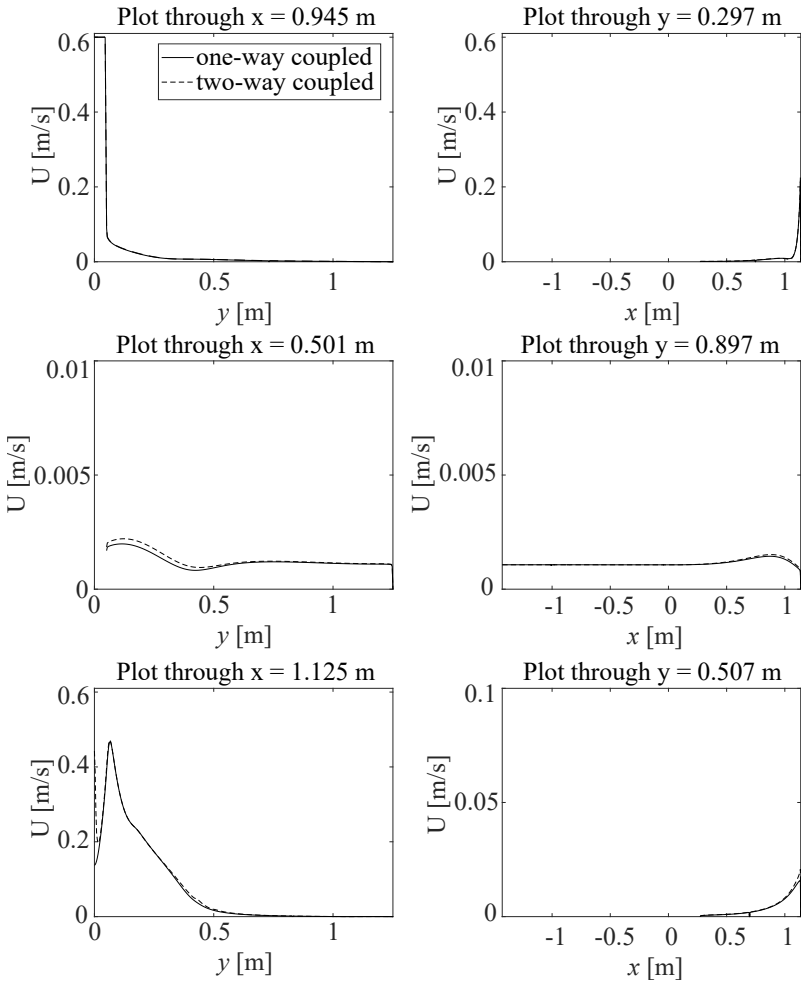

Figure 25: One- and two-way coupling simulation results, where the dotted line it the results of the two-way coupled simulation and the solid line is the results of the one-way coupled simulation.

A one-way coupled approach was considered appropriate for the simulations in this thesis, both due to minor differences in the velocity field and the computational cost. In the theory subsection 2.5 for particle flow modeling it is explained how the computational time can sometimes be a reason for preferring a one-way coupled setup. The two-way coupled simulation ran for approximately 72 hours, while the one-way coupled simulation ran for approximately 8 hours. Both simulations had over 44 million particles released at the end time and released 3021 particles every timestep. With the relatively minor changes in solutions and considering the computational time, a one-way coupled setup was decided to be sufficient for the purpose of this thesis.

The smallest half of the particles seems to be swirled in the bottom of the tank and their distribution is shown in Figure 26. This result represents the particle distribution when no recirculation pump is introduced to the system and 80 L of manure is flushed into the tank with a velocity of $0.6\,\mathrm{ms}^{-1}$ for 18 s. The different particle sizes are represented by a lighter color for the smallest particles and a darker color for increasing diameters. The resulting color scale for the particles is presented in Table 10 together with the number of particles in the parcels plotted and the resulting number of particles in the tank volume. From Figure 26 one may observe the five smallest particle diameters to be lifted and swirled. The heaviest particles do not leave the floor but are pushed along the floor towards the outer part of the tank. Due to no particle-particle interaction model, particles are overlapping in the plot. This is considered nonphysical behaviour and will be discussed in section 5.

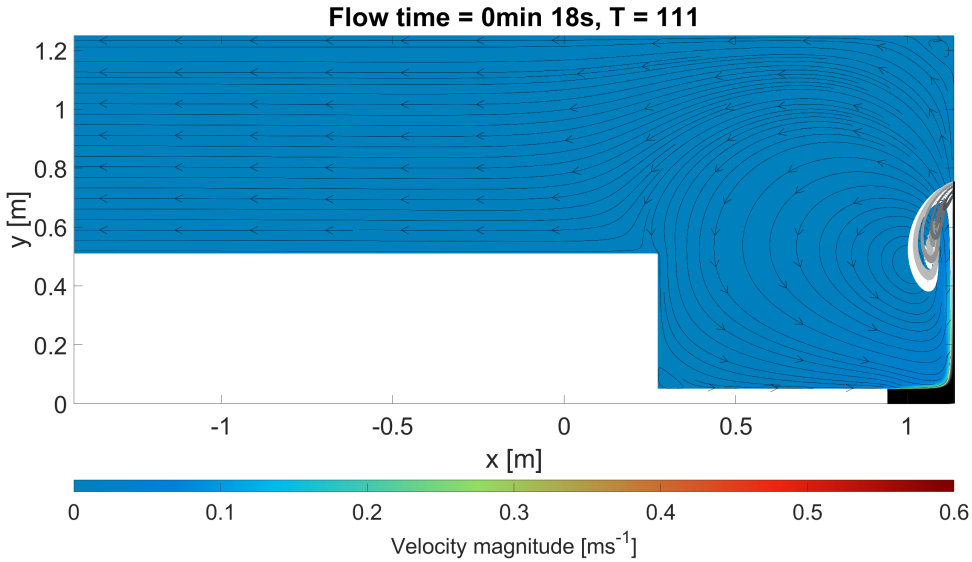

Figure 26: Particle plot showing the particle distribution after $T = 111$ when the inlet velocity is $0.6\,\mathrm{ms}^{-1}$. The different parcels are represented by different colors and the number of particles per parcel and the diameter of the particles are shown in Table 10.

Table 10: Specifics regarding the particles that were injected into the domain. The table provides the particle size and color to describe the particle plots in the subsection, as well as the number of particles in each parcel and the total number of injected particles.

Color of particle	Diameter of the particle [mm]	Number of particles in parcel	Number of particles in volume
	0.10	1017	585 713 670
	0.27	410.4	236 362 869
	0.43	251.1	144 653 300
	0.60	137.8	79 360 761
	0.77	56.16	32 347 716
	0.93	14.56	8 383 910
	1.1	2.060	1 186 493
	1.3	0.1360	78 323
	1.4	0.003537	2 038
	1.6	0.00003018	17

Figure 27 presents the particle distribution for the inlet velocity $U_{max} = 0.1\,\mathrm{ms}^{-1}$ showing less particles to be swirled when the velocity is decreased. This simulation reviles a decrease in force acting on the particles for reduced inlet velocity causing two of ten diameters to be lifted from the floor for $U_{max} = 0.1\,\mathrm{ms}^{-1}$. In contrast, five of ten diameters will be lifted and swirled for $U_{max} = 0.6\,\mathrm{ms}^{-1}$. In addition one may observe the larger particles to not be pushed along the floor in the same matter as described for $U_{max} = 0.6\,\mathrm{ms}^{-1}$. This is thus the reason for believing higher velocities to be preferable to lower velocities when mixing of new substrate is considered.

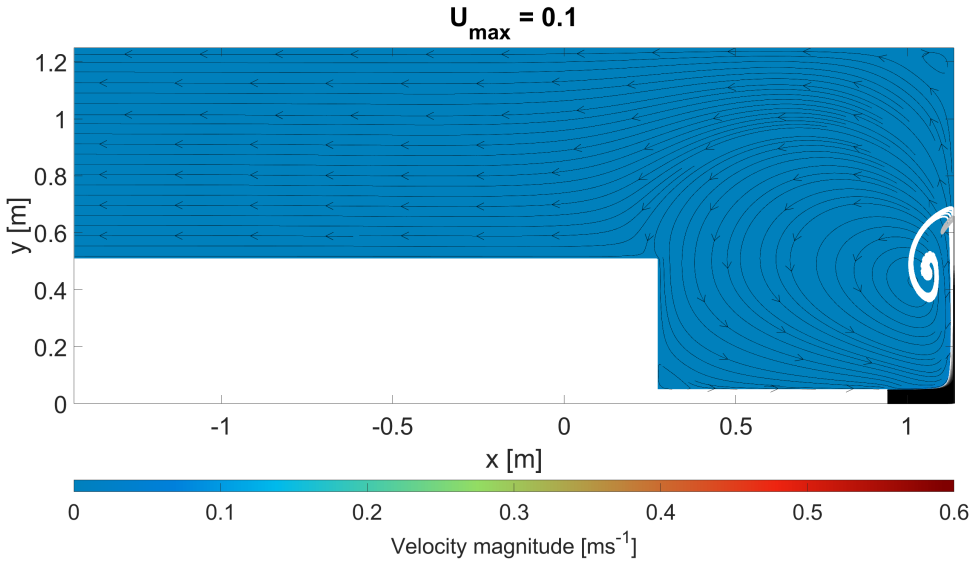

Figure 27: Particle plot showing the particle distribution after $T = 111$ when the inlet velocity is $0.1\,\mathrm{ms}^{-1}$. The different parcels are represented by different colors and the number of particles per parcel and the diameter of the particles are shown in Table 10.

Simulation of floating particles showed the density of the particles to be one of the main parameters influencing the particle paths. A simulation with floating particles was conducted because the density of the granules in nature will vary based on the internal gas production. The result from this simulation is presented in Figure 28. From the plot, one may observe particles being swirled by the main vortex. In contrast to the case with non-floating particles, the large particles are the particles moving with the greatest distance to the floor. The small particles are transported further in the radial direction in contrast to the large particles which mainly move axially. The intermediate particle diameters are then distributed between the small and large particle distributions. Figure 28 also shows a particle distribution covering a grater volume when compared to the non-floating particles in Figure 26. All things considered, the simulation of floating particles shows the particle density to be an important parameter for the particle paths.

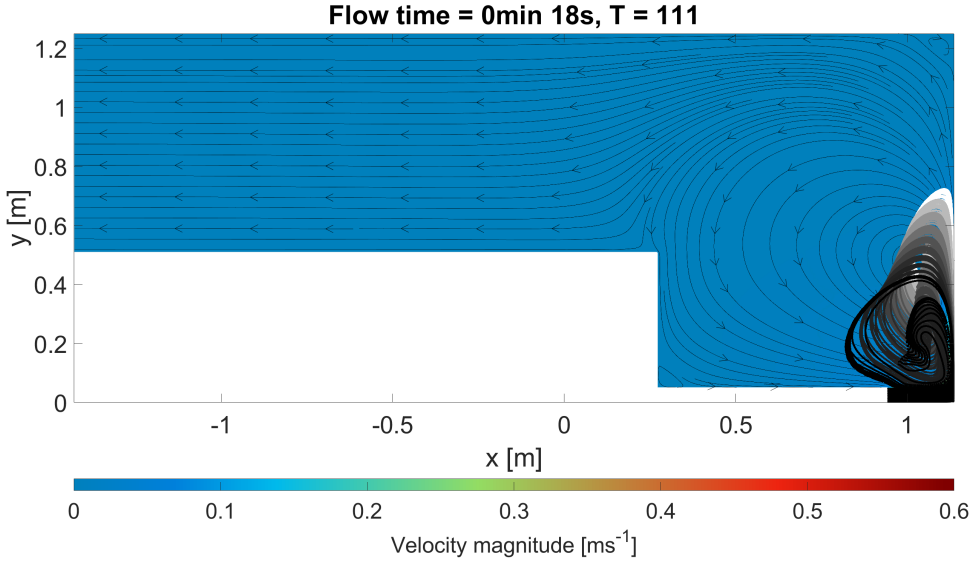

Figure 28: Particle plot showing the particle distribution in TR after $T = 111$ for particles of density less than the surrounding fluid. The parcels plotted are described in Table 10.

A simulation concerning the particle distribution in TR when using a recirculation pump was conducted, and the results reviled increased deviation of particles throughout the reactor volume when compared to no such recirculation. The particle distribution at $T = 1500$ is shown in Figure 29 and represents the particle distribution with the recommended pump duration described in subsection 4.3. The largest particles are collected at a singular point in the flow close to the recirculation zone of the corner. Because no particle-particle interaction model is activated, a nonphysical collection of the heaviest particles is to be found at this singularity. There are therefore only the three particle diameters of the smallest size, which are distributed to the rest of the domain. Most of the particles with the second and third smallest diameters are swirled by the main vortex in the tank. The smallest particles are mainly distributed among three different vortices. A large part is swirled by the main vortex as for the two larger diameters. Some particles are trapped in the recirculation zone in the corner of the tank, while the rest are swirled by the vortex forming on top of the main vortex. This shows the recirculation pump configuration used to cause the smallest particles to reach the upper third of the tank. Snapshots of the particle positions at earlier stages of the flow are presented in Appendix B and show how the particles are transported through the domain.

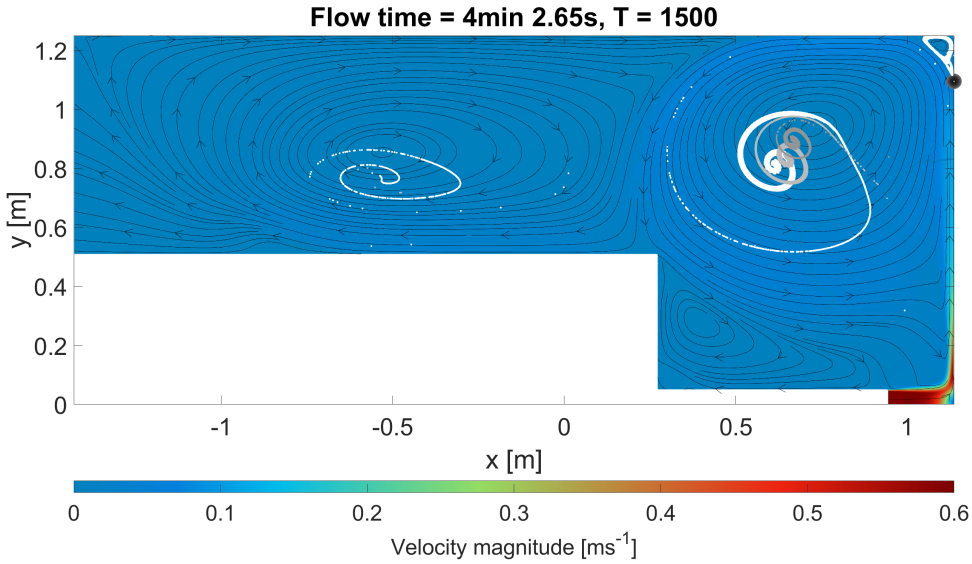

Figure 29: Particle plot showing the particle distribution in TR after $T = 1500$. The parcels plotted are described in Table 10.

When comparing Figure 29 to the real geometry of TR presented in Figure 5, the particles have still not reached the particle retention devices. In Figure 29, the inlet of the particle retention devices has been placed at approximately $x = -1\,\text{m}$, while the highest particle is placed at $x = -0.74\,\text{m}$. Given these points, there is reason to believe no particles from the incoming substrate will reach the inner tank of TR.

5 Discussion

This section discusses the limitations of the thesis's scope, methodology, and results in order to assess the plausibility of its findings. First, the limitations of the scope will be discussed to clarify the decisions made to achieve the thesis's objective within the allotted time frame and with the available data, resources, and facilities. The objective of the second section is to provide the reader with insight into how the simplifications and models used will impact the solution by examining the dependability of the methods and numerical values used to generate the simulated results. Finally, implementation of the findings and their anticipated impact on biogas production will be discussed. Each subsection of this section is therefore intended to explore how the findings of this

thesis can be utilized to develop recommendations for enhancing TR mixing to improve the biogas yield.

5.1 Limitations of the thesis

The scope of this thesis is limited to transient 2D simulations of TR, taking into account both single-phase and particle injection in order to find recommendations for improving the mixing in TR. This method was chosen due to the available information and the current stage of development for TR. The available information consisted of the results of the project described in section 1.1, some studies from USN regarding the biogas production and particle distribution from pig manure in TR, and operational experience from an early pilot facility. Because the biogas production at the pilot facility deviated significantly from the expected biogas yield from earlier lab studies at USN, the determination for whether mixing would increase the biogas yield was intriguing. Due to TR still being in the pilot phase of development, the geometry within the main tank is still evolving. Therefore, general recommendations were preferred, as this would be advantageous for the system's future development. Keeping this in mind, the scope was refined based on the fluid information provided for the system. USN analyzed pig manure and therefore provided a particle distribution. However, the flow field of TR was never investigated, and there was thus no experimental data available to validate the particle flow. As a result, a particle injection was determined adequate for simulating the injection of manure in order to observe whether the trends and suggestions from earlier simulations could be strengthened or confirmed.

Simulations in 3D were deemed out of scope for two primary reasons: high computational cost and lack of experimental data. The project described in section 1.1, 3 mm was determined to be an adequate spatial discretization level. With the volume of the TR tank being 10 m^3, the approximate number of elements in a 3D simulation would be approximately 370 million cells. This would be greater than a thousand times the number of elements in the extended mesh displayed in Figure 10 in subsection 3.3. Thus, a 3D simulation would have significantly increased the computation time. When there is no experimental data for the flow, there is no validation basis for the simulations, meaning there is no way to quantify the level of accuracy gained by running 3D simulations. The fact that TR's geometry changes between versions is also a challenge, which gives the simplified 2D geometry an advantage. In other words, the flow pattern caused by distributions such as support legs can be separated from the flow caused by the geometry of the tank when using 2D. Therefore, there is reason to believe that, despite the fact that 3D simulations are most likley to be more accurate when considering the exact flow pattern, the 2D simulation conducted in this thesis may provide information with sufficient accuracy based on the resources available and the industry's interest.

Due to the lack of test facilities and experimental setups, no practical investigation into the mixing was conducted. At the time this thesis was written, there were two pilot facilities producing biogas, but these had several operational issues and were therefore not suitable for testing. A lab-scale model with PIV measurements could have been useful for validating the simulation results, but such a model would have been time-consuming, so it was decided to be excluded due to the available time and lab facilities. In later sections, it will also be argued that the model for this thesis is appropriate for engineering purposes when flow specifics are unimportant.

Due to the lack of experimental data and the paucity of relevant literature, a case setup in which simulations would be compared and evaluated against each other were decided suitable. The geometry has a significant impact on turbulent startup flows, and due to the geometry of this thesis, similar flows were difficult to detect in literature searches. This could be due to the difficulties involved in measuring the velocities of transient and turbulent startup flows. In addition, there are few studies examining the mixing of a periodically fed UASB reactor in relation to the flow pattern in the tank. There are reasons to believe that the opacity of the sludge makes it difficult to obtain reliable results from such studies. As explained in the theory presented in subsection 2.1, the optimalization of mixing in such reactors is often associated with minimizing low velocity flow zones. However, it is possible that similar studies of periodically fed UASB reactors exist, but no such literature was discovered during the subject's literature search.

5.2 Method and numerics

The purpose of this second subsection of the discussion is to discuss the simulations' reliability, uncertainty, and errors. In the section 1.1 project, the setup of the turbulence model, the initial conditions, the mesh, and the boundary conditions were discussed. It was determined that simplifying the geometry and the fluid was necessary to obtain useful results within the allotted time frame. However, it is important to note that the model was not validated against experimental data and was only concluded to model the major flow characteristics. In this thesis, transient simulations, multiphase flow, and three-dimensional modeling have all been examined as suggestions for future research. As described previously, however, 3D simulations did not fall within the scope of this thesis. Transient particle simulations were of greater industrial interest than a more precise geometric model; consequently, the geometric simplifications were maintained. This section will continue by discussing the transient setup, the case study, and the particle phase modeling.

Calibration case

The calibration case was executed under the same conditions as the article by Yu et al. [23]. Nevertheless, there are notable differences between these two instances. Yu et al. investigated the vortex formation from an impinging jet in between two plates. This rendered the problem pseudo-two-dimensional and symmetric relative to the slit's center-line. In this thesis, an axisymmetric domain is employed, and the domain outlet varies. The outlet of this thesis' geometry will cause the vortex to develop from above, before being constrained by the walls of the tank. In the study by Yu et al., the vortex is limited by a wall from above but will develop freely sideways. The first four frames of the study were chosen because the upper wall was considered to have the least influence on the development of the flow during these frames. However, the $T = 10$ plots from Figure 11 and Figure 12 demonstrate the upper wall to have a significant impact on vortex formation. This might be concluded based on the vortex's center in this instance. In Figure 11, the vortex center is positioned above the inlet, which was not possible in the study by Yu et al. For later time steps, to compare the formation of the vortex is difficult, despite similarities indicating similar flow development. The similarities may be specified as the path of the vortex center and the radial length of development. Meaning, the vortex moves mainly in the axial direction before stagnation entails movement in the radial direction.

It is essential to remember the plot presented by Yu et al. where the vorticity is plotted as opposed to the plot of the velocity magnitude and flow streamlines. This was selected because of the difficulties of obtaining a vorticity plot illustrating the flow's characteristics. The vorticity of the system was plotted in grayscale, but there was no clear definition of how to calculate the vorticity. The article lacked labels or explanations on how to obtain the plots, so a different method of data presentation was chosen. However, a LES study [24] of similar geometry to TR obtained similar vorticity field plots when compared to the findings of Yu et al. This study appears to plot the vorticity of the flow to illustrate the formation of vortices using a filter, but the creation of these plots is not explained. Because vorticity describes local rotation, streamlines and the velocity magnitude plot were chosen to characterize vortex growth.

A more accurate calibration basis was attempted obtained, but literature concerning the initiation of such flows proved difficult to find. Startup flows are complicated to quantify and describe for large-scale turbulent problems. Consequently, there seems to be fewer articles concerning the subject. The geometry of this problem, which involves a submerged jet impinging a cylindrical chamber, has a significant effect on the flow, resulting in large disparity between the available studies of the subject. Therefore, a considerable amount of time was spent refining the search terms for the literature search. The two articles described [23, 24] were therefore deemed adequate for model calibration.

The objective of the residual analysis was to determine whether the obtained solution varied from the chosen residual criteria. This analysis revealed a residual criterion of 5×10^{-6} was required in order to obtain a solution that appeared to be independent of the criterion. This method for ensuring convergence is based on the assumption of the residuals of a convergent scheme to converge to zero as the time step and mesh size decrease. However, the discrete equation is iteratively solved,

which means, even though the discretization is infinitesimally small, the iteration must approach infinity for the residuals to become zero. Thus, a residual criterion is established to determine when a solution is deemed acceptable, thereby preventing an infinite iteration process. On the other hand, an excessively large residual criterion will stop the iterative process before the solution is deemed converged. Therefore, a sufficiently stringent criterion will result in a solution comparable to one obtained by reducing the criteria further. Due to the increase in computational time caused by additional iterations, it is desired to employ a restrictive criterion but not stricter. This trade-off between computational time and precision caused the simulations in this thesis to have residual criteria of 5×10^{-6}. In these simulations, the model and application uncertainties are regarded a larger source of error compared to the discretization and convergence errors.

Because the project's setup, assumptions, and models are described in section 1.1, the model and application uncertainties will not be examined in detail in this thesis. The model was conducted verified, but it has yet to be validated due to a lack of experimental data. However, the model is assumed to describe the flow trends, and was therefore considered suitable for engineering purposes. This thesis will only cover the newly introduced properties not examined in the steady state project. On the other hand, there is a possibility that the inaccuracy in the previously accepted model was inaccurate. However, this calibration demonstrates flow trends to still be predicted effectively and accurately for engineering purposes. Therefore, the simulations in this thesis are compared under the assumption for the system to exhibit similar behavior.

Case study

The purpose of the case study was to determine whether it was possible to generalize the effects of velocity, distance from the inlet, and the use of a stagnation plate on the mixing in the tank. This information is crucial at this stage of development for the technology because it allows TT to make informed adjustments to the tank. Therefore, the focus of the case study has been to describe how adjustments may be made. Additional case combinations that were not explored in this case study may have revealed different elements and, as a result, led to different recommendations. In contrast, the purpose of this study is to examine the effect of modifying one of the parameters. Therefore, the same results is implicitly assumed reordered parameter changes. It is possible to argue the assumption to be valid, given the reason for the modifications of parameters. Frequently, the reason for intending to alter the geometry will determine the scope of the modifications. When selecting a pump, for instance, the velocity will be modified based on the pump's working area. Then, based on the working regime of the pump, it will be intriguing to determine the velocity. Typically, the distance to the floor will be adjusted to prevent obstruction of the inlet area. To exemplify, this could be a distance, adjusted based on the substrate used at sight. The plate cases were examined due to an early version of TR. Originally, this plate was inserted into the tank due to a screw mechanism at the tank's base. However, this was reconsidered, and it was therefore intriguing to determine whether it was desirable to retain the plate.

The cases were selected subjectively to meet the objectives of the case study; consequently, the results may be influenced by this selection. In order to investigate the effect of changing the inlet velocity, Cases 1-3 were designed with three distinct velocities. Based on the pump duration displayed in Figure 9 from subsection 3.2, Case 1 velocity was intended to represent low velocity. Case 2 was selected as an intermediate case with relatively high velocity and low pump duration, while Case 3 was selected to represent high velocity. The results of these simulations are therefore only discussed in terms of how the velocity affects the flow; the effect of changing the time discretization accordingly, is not discussed, as it is dependent on the CFL-condition from Equation 25 in subsection 2.6. With converging solutions and comparable results for the streamlines and flow development, this change in discretization was therefore accepted without further investigation. However, the possibility for this to happen is present, although the likelihood is considered small. Cases 4–9 were chosen to examine the effect of geometrical modifications, and a new mesh was employed for each case. The spatial discretization of these cases may therefore be a source of error. Nonetheless, the selected cases demonstrate reasonable results, and the flow trends are discernible in all cases compared. The mesh is not discussed in detail in this thesis due to the verification ot the mesh cinducted in the steady state project described in section 1.1. In addition, the effect

of modifying the geometry and, consequently, the mesh is considered a negligible source of error based on the calibration.

Recirculation pump

A recirculation pump was discussed as a possible solution to improve the mixing after comparing the simulation results of Case 3 with the steady state results found in previous work.Figure 2 in section 1.1 illustrates the flow zones of TR in the case of steady state caused by continuous flow at the inlet. Comparing Figure 1 and Case 3 in Figure 15 reveals flow field of Case 3 not to be fully developed. A decreased velocity magnitude across the volume is the observation causing this assertion. Therefore, there was reason to believe increased pump duration to improve the tank's mixing.

To estimate the duration of the recirculation pump, Case 3 was run for 62,400 time steps and the solution was extracted every 600 time steps. In subsection 4.3, the snapshots for $T = 370$, $T = 740$, $T = 1100$, $T = 1500$, and $T = 1900$ were presented, and $T = 1500$ was determined to be an adequate duration for the pump. The change in flow zones when comparing the snapshots together with the steady state solution shown in Figure 2 in section 1.1 was the main reasons for this decision. When $T = 1500$ is reached, the bottom third of the tank has developed a large velocity zone. This solution shows similarities with the established steady state solution. When simulating until $T = 1800$, minor changes in the flow zones are observed. Therefore, the expected gain for increased pump duration after $T = 1500$ is considered minor. It is important to note, $T = 1500$ is not to be determined by objective stopping criteria. For this reason, the given time should be considered a factor of magnitude. Meaning another optimal duration for the pump may be found, but after $T = 1500$, simulations indicate negligible effects for the mixing effect. Based on the uncertainties in the modeling of the system and the subjective stopping criteria, $T = 1500$ may be calculated in real time in seconds when the inlet velocity is determined, and may be used as an order-of-magnitude factor in determining pump duration. Such a practical study for determining the duration of a recirculation pump should be conducted to validate the findings of this thesis and to derive a pump duration recommendation.

Particle injections

A distribution of particles covering a large fraction of the volume in TR was preferable, particle injection simulations were therefore conducted to address expected increase in biogas yield for the studied cases. Due to the opaque nature of the manure, it is difficult to experimentally study both the flow and the injected particles. Such a setup would have been time-consuming and challenging to implement. Therefore, CFD was determined to provide insight to whether the particles in the tank were sufficiently distributed. This is despite the absence of experimental data to validate the results of simulations. Verification and validation of the particle injections are therefore consequently restricted to the selection of modeling.

The system's one-way or two-way coupling was selected based on simulation results obtained by running the setup with both coupling options until $T = 75$. Because of difficulties connected to the estimate of Stokes numbers for the flow, this method was chosen to be sufficient. The density difference between the granule phase and the continuous phase is considered to be relatively small. A Stokes number approaching unity is reasonable to assume. Therefore, a test was required to determine whether the simulations required a two-way coupled setup. It is essential to remember all flows to be two-way coupled. This is because, even though there are small particles with no difference in density compared to the continuous phase, the flow close to the particle will always differ from the flow without such particles. The particles will then follow the streamlines of the flow, but the flow pattern will change close to the particle's surface. The flow investigated in this thesis is, on the other hand, considered a small-particle flow whose density varies. Consequently, the outcome of the simulation indicate a need for coupled modeling in both directions. In some regions, the streamlines are not overlapping, indicating minor alterations in the flow pattern. For two-way coupling, this will cause the particles to be transported along a slightly different path.

This is depicted in the particle plot in Figure 24, which depicts the small difference in particle position between the two simulations. There is reason to believe the differences in streamlines for these simulations' snapshots, to propagate and cause subsequent snapshots to differ as well. A second indication for two-way coupling is found by examining the velocity profiles. Figure 25 demonstrates the trend stated by the streamlines. Based on the slightly less developed particle positions in the two-way coupled simulation, the difference in velocity magnitude may be concluded to be significant. It is essential to remember that the uncertainty in viscosity and the assumption of Newtonian fluid flow are likely to result in a greater change in streamlines than the assumption of one-way coupling. In light of this, one-way coupling was selected due to the substantial additional computational cost associated with two-way coupling.

The need for physical models for the discrete phase was investigated in a similar way to the coupling by enabling the relevant models to observe the effect. Because the heat transfer in the system was determined to be out of scope, none of the physical models concerning such effects were included. Neither stochastic collision nor coalescence was enabled because the gas phase of the system is not modelled. The gas production's influence on the flow is however, not negligible, and is considered outside of the scope of this thesis. Henceforth, virtual mass force, pressure gradient effects, and DEM collision modeling were the only physical models considered in the modeling of the particle flow. Due to the ratio between the density of the continuous phase and the granules, virtual mass force and pressure gradient effects were enabled. Because of the flow acceleration appearing when a particle density is sufficiently higher than the density of the continuous phase, Fluent recommends in their theory guide [22], enabling virtual mass force and pressure gradient effects for density ratios exceeding 0.1. However, the ratio is below unity, and the simulation results when enabling this option are close to unchanged compared to no such modeling. The computational demand was, on the other hand, not significantly increased by this modeling and was therefore kept as a part of the model. The DEM collision was not a part of the model. However, the simulation results showed overlapping particle positions. Therefore, there is reason to believe DEM to be necessary to find a more accurate solution. On the other hand, the simulations were conducted without any experimental data for validating the particle flow, hence the results were treated with statistical interest. This means, the likelihood of finding a particle is increased in the case of overlapping particles. An important side to the argumentation is on the other hand the non-modeled particles already existing in the volume. The collision between particles in the volume would therefore have been inaccurate either way, and the result of this simple model was therefore accepted without DEM collision modelling.

Due to the absence of DEM collision modeling and the use of one-way coupling, an exact volume flow representation of the particles is unnecessary. This is the case because neither the particles nor the flow affects the presence of the particles. Thus, the particle track and distribution will be independent of the volume's particle concentration. In other words, the solution in this instance is independent of the total particle flow rate. This is the reason for not verifying the number of particles injected into the volume. When enhancing the model to include a particle collision model, it is necessary to verify and investigate such specifics to ensure accurate results.

Granules were modeled using a spherical approximation, although this is inaccurate. Tassew et al. [15] examined how to estimate the terminal velocity of granular pig manure and concluded the granules to be non-spherical and require a shape factor in order to be treated as spheres. As a result, drag on the particles cannot be accurately predicted when spheres are assumed. Some particles, for instance, have a large perimeter-to-volume ratio, causing the granule's surface to wrinkle. In many instances, this will increase the drag compared to a sphere of the same volume. In contrast, the shapes of the granules will vary significantly, resulting in granule shapes with less drag than a sphere. One such shape is the droplet shape, which frequently resembles a streamline and would therefore be exposed to less drag due to late separation. However, the particles is not described by Tassew et al. according to drag affection, causing visual description of the particle shapes to be the information available for shape factor calculations. Visual data collected about the granules indicates the top and fresh granules to be more spherical compared to the granules collected from the remainder of the reactor. In the simulations, a spherical approximation was deemed acceptable due to a lack of information required to calculate an appropriate shape factor for the granules.

The particle representation in the results is based on Fluent's parcel representation. Therefore, the particle representation is essential to address. Every timestep, Fluent injects one parcel of each diameter from each cell face at the inlet. Consequently, the number of parcels in each diameter fraction is constant and independent of the particle distribution. Nonetheless, a parcel containing the largest diameter will only contain a small fraction of the particle. In contrast, a parcel containing particles of small diameters will represent multiple particles. This may be interpreted as a statistical representation of particle placement, i.e., the likelihood of fining a large particle will increase in areas of multiple large particle parcels. This demonstrates the injection of fresh manure differs from the simulated injection. The particle distribution at a single snapshot is not expected to contain particles of all sizes. The injection of manure will indeed be different for every new batch flushed. A recreation of the exact conditions is therefore difficult to obtain. To model the inflow using parcels with the Rosin-Rammler distribution is therefore regarded as representative for the particle distribution.

5.3 Applications and biogas yield

This subsection discusses the applications for the results and their potential increase in biogas yield. The objective is to relate the findings of this thesis to the biogas theory presented in subsection 2.1. The case study will be discussed by relating theory, simulation results, and operational experience to provide a foundation for the inlet velocity and geometry recommendations. Further, the recirculation pump results will be discussed to provide information regarding the expected improvement of the system using such an installation. Finally, the simulations of particle injection will be discussed in order to describe how the particle distribution may be related to the biogas yield. The intention is to elucidate the adjustments to the system for exhibiting the indications for increasing the biogas yield.

Case study

The case study was conducted due to TR still being in the process of development and optimization, thus changes to geometry and setup are frequently discussed. When alterations are made to the geometry or inlet parameters, comprehension and optimization need to be addressed to determine the modification's effect. Consequently, the cases were selected based on the previously discussed geometry and property modifications. The objective was to determine whether generalizations about preferred geometry and velocity changes could be made based on the expected advantage for increased biogas yield.

Case 1–3 examines the effect of varying the velocity to comprehend how the mixing conditions are affected. The simulation of Case 1-3 demonstrates the inlet velocity to have no effect on the flow pattern when adjustments of the pump duration are made. The expression for T may be written as a function only dependent on the heat exchanger volume and the inlet diameter. Therefore, when a change in flow pattern is desired, two options for achieving a more developed flow are available. The first option is to reduce the inlet's diameter. T is inversely proportional to D^3, meaning small change in D will have a significant impact on T. For instance, a ten percent decrease in diameter results in a forty percent increase in T. There are, however, operational and production reasons for the given inlet diameter, making a reduction in this property undesirable. Because clogging has been an issue in some locations, a pipe with a diameter of 110 mm was chosen for the inlet. The second option for increasing T is to increase the volume inserted to the tank ever flushing period. However, as described in subsection 2.2, the volume of the heat exchanger is determined by the required HRT and pump frequency. A larger quantity of substrate flushing into the tank will therefore either decrease the HRT or frequency. As described in subsection 2.1, a decrease in HRT may result in accumulation of acids, which further may cause the process to fail. In order to maintain constant HRT, the pumping frequency may be decreased. When the pumping frequency is decreased, the new substrate may not be able to stir the tank's bottom layer as desired due to settling. Utilizing a recirculation pump is one way to increase T without increasing the volume of the heat exchanger. After the new substrate has been injected, some of the substrate in the tank is recirculated back into the tank. This will result in a more developed flow within the tank without

affecting the inlet diameter, HRT, or pumping frequency.

Case 3 was deemed superior when investigating Case 1-3. In the scientific literature, mixing is typically linked to kinetic energy and the mixing zones described in subsection 2.1. This indicates areas of widely spread kinetic energy to be preferred when compared to small areas of high kinetic energy. Therefore, despite the fact for the development to be independent of the inlet velocity, will higher velocities be preferred. A greater force acts onto the particles and the surrounding fluid when the velocity is high. Consequently, kinetic energy is frequently used as a measurement of effective mixing, and this is proportional to the square of the velocity magnitude. In other words, doubling the velocity at a point quadruples the kinetic energy at the same point. Case 3 has the highest inlet velocity of the three cases and was therefore deemed the optimal option. It is nonetheless essential to remember $Umax = 0.6\,\mathrm{ms}^{-1}$ to not necessarily be the recommended inlet velocity. Case 3 represents high velocity and does therefore indicate high velocity to be used when a pump is installed.

Recommendations for the distance from the inlet to the floor were investigated through Case 4-6. When comparing four sizes of L between $2D$ and $5D$, the differences were negligible. The velocity magnitude along the floor is large for $L = 2D$ compared to $L = 5D$. Flushing against the floor is assumed desirable because of the heaviest particles nature to settle at the bottom of the tank [15]. However, the changes in velocity magnitude along the floor are minor when comparing the cases indicating the distance to be determined by other factors. Case 3-6 demonstrates that a shorter L would be preferred if there are no operational or production-related parameters crucial to this length. Nonetheless, $L = 2D$ should not be treated as the recommended length. This distance is merely an example of how decreasing the distance will affect mixing. The recommendation is therefore to prefer a relatively short distance from the heat exchanger outlet to the floor.

In Case 7-9, a plate was introduced into the flow to investigate its impact on the flow pattern and mixing. The plate causes a new recirculation zone to appear under the plate, but the over all flow pattern is similar to the other cases studied. This indicates the plate to disrupt the flow, causing a portion of kinetic energy to be distributed under the plate, while the majority of the kinetic energy is distributed in a similar manner to earlier cases. The disadvantage of the plate seems to be the zone of the floor where the particles are never stirred. However, this is a small volume of the tank, and the plate may be considered a component of the tank whenever it serves a functional purpose. A simple geometry emerges as the optimal option for tank mixing. This is again due to the assumption of preferable high velocity along the tank's floor.

Recirculation pump

A recirculation pump will be able to extend the pump's runtime without diminishing the system's HRT. According to the theory of subsection 2.1, the HRT is a sensitive and essential factor when optimizing a biogas reactor. A recirculation pump will make the mixing of the reactor volume independent of the HRT of the system. A recirculation pump circulates a portion of the existing fluid in the tank back through the inlet. This will not decrease the HRT because the same amount of fluid is extracted as is flushed through the inlet; therefore, the volume flow out of the system is zero.

Although the mixing in the tank is of interest, it is essential to remember the aim for an increased biogas yield. With this intent, the total energy balance of the system becomes implicitly a limitation for the pump duration. Whenever increasing the pump duration consumes more energy than the increased biogas yield provides, the system's net energy output will decrease. This is a crucial consideration when introducing a recirculation pump to the system. However, due to the lack of experimental data concerning the system's energy balance, this consideration of energy was deemed out of scope. To address the systems energy balance, an experiment investigating the relation between biogas yield and pump duration will be recommended before introducing a recirculation pump to the system. Moreover, the results from the simulations of the recirculation pump are relevant to this experiment because of the indication for time-related aspects.

The inlet for the recirculated substrate must be addressed when introducing a recirculation pump

into the TR system. This inlet will disrupt the flow pattern in TR, but may contribute to the mixing effects. The recirculation pump will remove substrate from the tank at the same volume flow required at the inlet of TR. In other words, the recirculation pump will add an outlet to the volume of the tank, which may alter the flow pattern and improve mixing. This effect was deemed out of scope, but differences concerning the flow pattern may be large and are therefore important to address.

Particle injections

The primary reason for investigating the flow pattern within TR is to determine whether or not there are reasons to suspect minor system modifications to increase biogas production. Some aspects of the flow are overlooked when only the flow pattern is considered. Because the majority of biogas potential in manure resides in solids, the distribution of this material is closely related to biogas production. The primary argument for using the previously described flow zones is the likelihood linked to high velocity zones capability to distribute particles throughout the volume. However, because particle distribution frequently deviates from streamlines due to differences in density, a particle simulation may reveal different aspects than flow zone analysis. Particle simulations were conducted to determine whether there was reason to believe a recirculation pump to increase the biogas yield. This subsection will discuss how these simulations may be used to comprehend and enhance the biogas yield from TR.

In this thesis's analysis of TR the dispersion of the particles is the main indicator of biogas production. Simulations indicate only small particles to be lifted from the floor in TR. This is because the flow force acting on the larger particles in the axial direction is less than the gravitational force. Therefore, would a larger force on the particle be required to lift the particles of large dimensions. However, the simulations demonstrate nonphysical behavior with overlapping particles, indicating the positions of the particles deviate from simulation results. Given a deviation of heavy particle positions, it is plausible to assume a change in force distribution acting on the particle to be likely. This may result in swirling of the heavy particles. On the other hand, there is reason to believe the heavy particles to quickly settle, making the proposed distribution likely.

Another aspect of the dispersion of particles is the settling and particle distribution in the period of no pumping. Even though there is no injection of energy to the system will the dissipation of the injected energy still affect the flow. This causes the particles to continue moving towards the sidewall despite the flow being dominated by the velocity dissipation. Therefore, is there reason to believe the particles to be dispersed throughout TR's floor. This effect will not, however, improve the axial particle distribution. Thus, the incoming particles are dispersed over a small volume, and it is plausible for the digestion of the new substrate in TR to be slower than feasible.

To enhance the dispersion of particles and, consequently, the mixing, velocity may be regarded as an essential factor. As stated previously, the change in velocity has no effect on the degree of flow development, but particle simulations indicate the impact to be significant when considering the number of swirled particles. For the results shown in Figure 27, where $Umax = 0.1\,\mathrm{ms}^{-1}$, only two out of ten particle diameters were swirled. In comparison, this number is five out of ten for $U_{max} = 0.6\,\mathrm{ms}^{-1}$. As described, this factor is significant because of the increased external force acting on the particle. This can be detected explicitly in the particle momentum balance in Equation 20 from subsection 2.5, in which the velocity field, $\mathbf{U}$, is proportional to the drag force acting on the particle. An increase in $\mathbf{U}$ will cause an increase in the force acting on the particle, assuming that density, gravitation, and external forces remain constant. However, it is necessary to consider the additional power cost when higher acceleration is demanded for increasing the inlet manure's velocity. When selecting a feeding pump for TR, it is important to consider the increase in biogas yield caused by higher velocity. Given these factors, the general recommendation will be to favor high inlet velocity when mixing is the primary concern.

Density differences in the particles are a crucial aspect of biogas production. Particles with different densities will move along distinct paths and produce a constant transient system. The simulation results revealed a significant difference in particle motion as the granule density decreased. This is significant because the granules in the system naturally variate in density due to the internal

production gas. As described in the theory section subsection 2.1, this variation in density will cause some granules to rise. This fluctuating density is not accounted for in this thesis' simulations. The reason for this simplification may, however, justify based on this effect to be less pronounced for incoming substrates due to internal biogas production in fresh manure. On the other hand, it is essential to remember that the path of a particle is strongly influenced by its density. Therefore, the simulations demonstrate how low-density particles will move relative to high-density particles. On the basis of the findings of Tassew et al. [15], the majority of particles in fresh manure will be high-density particles, but lighter particles will also be present. Even though only a small fraction of the particles will follow the exact path, the streamlines provide a consistent indication of the overall flow in the reactor. Overall, the particle motion in TR is complex, and the particle simulations do not attempt to describe this dynamic; rather, they provide insight into how particles are influenced by the fluid flow.

Recirculation simulations demonstrated an increase in high-velocity zones causing the interest for understanding how particles are affected by such a change. The resultant particle flow simulation confirmed the hypothesis of increasing high-speed zones to result in improved particle distribution. When recirculation was used, the particles were increasingly dispersed across the volume of the tank. In terms of lifting the heaviest particles, increasing the pumping time do not appear to be an effective strategy. On the other hand, the heaviest particles are concentrated at a singular point of the flow, non-physical behaviour thus indicate the heavy particles to be distributed in other ways than suggested by the simulations. There will likely be a buildup of particles in this corner over time. This buildup is not necessarily undesirable, the settling will cause the corner to round off, allowing the domain to be more streamlined. At this point, the incoming fluid will be transported without accumulating in the recirculation zone, likely resulting in improved particle mixing. There is reason to believe biogas production is more efficient whenever a recirculation pump is included in the system.

6 Conclusion

The aim of this thesis was to understand how the incoming substrate is mixed in TR by using ANSYS Fluent to perform CFD simulations for the purpose of finding recommendations for improving the mixing in TR. The CFD models employed in this thesis are considered to have a high degree of uncertainty, yet they were approved for engineering purposes owing to a lack of experimental evidence on the issue. This indicates the plausibility of the obtained simulation results to deviate from the actual flow pattern, but similar trends are anticipated. The high level of uncertainty is mostly related to the omission of biochemical reactions, the assumption of Newtonian fluid properties, the simplification of geometry, and the absence of a validation foundation. Therefore, flow details are not considered sufficient for making conclusive suggestions. Despite this, global trends of the flow are regarded sufficient for concluding recommendations. Thus, the following recommendations are made to improve the mixing in TR:

- High velocity seems to be beneficial to mixing and a feed pump for the system should be chosen accordingly.
- Flushing along the floor and a simple geometry should be pursued to reduce the risk of plugging and increase the force exerted on the heaviest particles settling to the floor of TR.
- A recirculation pump should be considered for enhancing the mixing and distribution of fresh substrate to TR.

However, it is essential to keep in mind that these recommendations aim to increase TR's energy surplus. Increasing the inlet velocity or incorporating a recirculation pump will increase the system's energy demand. Therefore, these recommendations are based on the assumption that the increased energy surplus resulting from an increase in biogas yield is greater than the system's increased energy demand.

7 Suggestions for further work

Two out of three recommendations made in this thesis involve increasing the energy input of the TR system. However, this is only sustainable when the increased biogas yield exceeds the increased energy demand. Therefore, energy analysis of a pilot facility is suggested for future work. Tests for increased inlet velocity and recirculation pump duration may be conducted to confirm the results of this thesis by examining the increased inlet velocity and recirculation pump duration. The results of such a study will most likely be influenced by the manure used on-site, but there is reason to believe that the same trends will be observed for different manure mixtures. However, the optimal duration and velocity will be unique to the tested facility, but may serve as a guide for other facilities.

By varying the velocity and measuring the biogas yield over a given period of time, the expected increase in biogas yield caused by an increase in velocity may be determined. Additionally, it is essential to measure the increased energy demand alongside the biogas yield in order to determine the gain caused by the velocity increase.

For the recirculation pump, a similar strategy is proposed to determine whether increasing the pump duration increases the biogas yield to the point where it exceeds the increased power demand. Another important key point in need of investigation is the intake for recirculation. Before a recirculation pump is added to the TR system, this intake should also be discussed and tested, as it is not considered in this thesis.

References

[1] 'Transforming our World: the 2030 Agenda for Sustainable Development'. eng. In: *Civil Engineering : Magazine of the South African Institution of Civil Engineering* 24.1 (2016), p. 26. ISSN: 1021-2000.

[2] Juan F Cisneros et al. 'Hydrodynamic evaluation of five influent distribution systems in a cylindrical UASB reactor using CFD simulations'. eng. In: *Water (Basel)* 13.21 (2021), p. 3141. ISSN: 2073-4441.

[3] Muhammad Asif Latif et al. 'Integrated application of upflow anaerobic sludge blanket reactor for the treatment of wastewaters'. eng. In: *Water research (Oxford)* 45.16 (2011), pp. 4683–4699. ISSN: 0043-1354.

[4] Yu Liu et al. 'Mechanisms and models for anaerobic granulation in upflow anaerobic sludge blanket reactor'. eng. In: *Water research (Oxford)* 37.3 (2003), pp. 661–673. ISSN: 0043-1354.

[5] Yong-Jin Chang, Naomichi Nishio and Shiro Nagai. 'Characteristics of granular methanogenic sludge grown on phenol synthetic medium and methanogenic fermentation of phenolic wastewater in a UASB reactor'. eng. In: *Journal of fermentation and bioengineering* 79.4 (1995), pp. 348–353. ISSN: 0922-338X.

[6] Shiplu Sarker et al. 'A review of the role of critical parameters in the design and operation of biogas production plants'. eng. In: *Applied sciences* 9.9 (2019), p. 1915. ISSN: 2076-3417.

[7] Yohannis Mitiku Tobo et al. 'Partial integration of ADM1 into CFD: Understanding the impact of diffusion on anaerobic digestion mixing'. eng. In: *Water science and technology* 81.8 (2020), pp. 1658–1667. ISSN: 0273-1223.

[8] Kristine Midtbø. 'CFD simulation of the mixing zones in a UASB biogas reactor'. eng. In: (2021).

[9] Binxin Wu and Shulin Chen. 'CFD simulation of non-Newtonian fluid flow in anaerobic digesters'. eng. In: *Biotechnology and bioengineering* 99.3 (2008), pp. 700–711. ISSN: 0006-3592.

[10] Caroline M Plugge. 'Biogas'. eng. In: *Microbial biotechnology* 10.5 (2017), pp. 1128–1130. ISSN: 1751-7915.

[11] Dieter Deublein and Angelika Steinhauser. *Biogas from Waste and Renewable Resources: An Introduction*. eng. Weinheim: John Wiley and Sons, Incorporated, 2010, pp. 101–109. ISBN: 3527327983.

[12] Ismail M Nasir, Tinia I Mohd Ghazi and Rozita Omar. 'Anaerobic digestion technology in livestock manure treatment for biogas production: A review'. eng. In: *Engineering in life sciences* 12.3 (2012), pp. 258–269. ISSN: 1618-0240.

[13] Khursheed Karim et al. 'Anaerobic digestion of animal waste: Effect of mode of mixing'. eng. In: *Water research (Oxford)* 39.15 (2005), pp. 3597–3606. ISSN: 0043-1354.

[14] Zohaib Ur Rehman Afridi, Wu Jing and Hassan Younas. 'Biogas production and fundamental mass transfer mechanism in anaerobic granular sludge'. eng. In: *Sustainability (Basel, Switzerland)* 11.16 (2019), p. 4443. ISSN: 2071-1050.

[15] Fasil A Tassew et al. 'Settling velocity and size distribution measurement of anaerobic granular sludge using microscopic image analysis'. eng. In: *Journal of microbiological methods* 159 (2019), pp. 81–90. ISSN: 0167-7012.

[16] Jun Wang et al. 'A review on CFD simulating method for biogas fermentation material fluid'. eng. In: *Renewable & sustainable energy reviews* 97 (2018), pp. 64–73. ISSN: 1364-0321.

[17] Wenche Hennie Bergland et al. 'High rate manure supernatant digestion'. eng. In: *Water research (Oxford)* 76 (2015), pp. 1–9. ISSN: 0043-1354.

[18] F. R Menter. 'Two-equation eddy-viscosity turbulence models for engineering applications'. eng. In: *AIAA journal* 32.8 (1994), pp. 1598–1605. ISSN: 0001-1452.

[19] Z Zhang and Q Chen. 'Comparison of the Eulerian and Lagrangian methods for predicting particle transport in enclosed spaces'. eng. In: *Atmospheric environment (1994)* 41.25 (2007), pp. 5236–5248. ISSN: 1352-2310.

[20] Michael Casey and Torsten Wintergerste. 'Best practice guidelines'. eng. In: (2000).

[21] Ismail B Celik et al. 'Procedure for Estimation and Reporting of Uncertainty Due to Discretization in CFD Applications'. eng. In: *Journal of fluids engineering* 130.7 (2008), pp. 0780011–0780014. ISSN: 0098-2202.

[22] ANSYS. *ANSYS Fluent Theory Guide*. Jan. 2021. URL: https://ansyshelp.ansys.com/account/secured?returnurl=/Views/Secured/corp/v211/en/flu_th/flu_th.html.

[23] Mingzhou Yu et al. 'Large eddy simulation of coherent structure of impinging jet'. eng. In: *Journal of thermal science* 14.2 (2005), pp. 150–155. ISSN: 1003-2169.

[24] Jonatas Emmanuel Borges et al. 'Large-eddy simulation of downhole flow: The effects of flow and rotation rates'. eng. In: *Canadian journal of chemical engineering* 99.1 (2021), S751–S770. ISSN: 0008-4034.

Appendix

List of appendices:

A Simulation log

B Recirculation pump snapshots of particles in TR

A Simulation log

Number	Case	Dx [mm]	Dt [s]	Velocity [ms^{-1}]	Simulation time [s]	Number of time iterations	Number of iterations	Residual criteria	Comments	Sim. Time
0	Validation	3	0.035	0.077	172		200	1.00E-03	Wrong D	
1	Validation	6	0.077	0.077	172	2234	200	1.00E-03	Wrong D	
2	1	6	0.014	0.419	20	1397	200	1.00E-04	Wrong D	
2.1	1	6	0.014	0	21	1500	200	1.00E-04	IC = end time @ Sim2	
3	Validation	6	0.068	0.088	152	2225	200	1.00E-04		
4	Validation	6	0.068	0.088	152	2225	200	1.00E-04	Smaller domain. vorticity tracing monitor points	
5	Validation	6	0.067	0.088	152	2269	400	1.00E-04		
6	Validation	6	0.067	0.088	132	1975	1000	1.00E-05	New color scale for vorticity plot	
7	Validation	6	0.067	0.088	132	1975	1000	1.00E-04	Monitor points conv. Crit.	
8	Validation	6	0.067	0.088	132	1975	1000	1.00E-04	Conv. Crit. Monitor points 0.0009	
9	Validation	6	0.067	0.088		1646	1000	1.00E-04	Monitoring the stream function	
10	Validation	6	0.067	0.088	132	1975	1000	1.00E-04	Plot of velocity in monitor points to validation	
11	Validation	3	0.034	0.088	132	3883	1000	1.00E-04		
12	Validation	3	0.029	0.088	132	4500	1000	1.00E-04		
13	Validation	3	0.034	0.088	132	3883	2000	1.00E-05	Animation simulation	
14	Validation	3	0.034	0.088	132	3883	2000	5.00E-05	Validation of residual criteria	

Table continued from previous page

15	Validation	3	0.034	0.088	132	3883	5000	5.00E-06	Validation of residual criteria. First time step did not converge (res. 9e-6) Animation every 600 time step.	
16	1	3	0.03	0.1	108	3600	5000	5.00E-06	1.-2. step did not converge (res. 7e-6)	08:45:00
17	2	3	0.012	0.25	43	3583	5000	5.00E-06	Animation every 600 time step.	07:27:00
18	3	3	0.005	0.6	18	3600	5000	5.00E-06	Animation every 600 time step.	05:40:00
19	4	3	0.005	0.6	18	3600	5000	5.00E-06	Animation every 600 time step.	05:41:00
20	5	3	0.005	0.6	18	3600	5000	5.00E-06	Animation every 600 time step.	06:01:00
21	6	3	0.005	0.6	18	3600	5000	5.00E-06	Animation every 600 time step.	05:58:00
22	7	3	0.005	0.6	18	3600	5000	5.00E-06	Animation every 600 time step.	
23	8	3	0.005	0.6	18	3600	5000	5.00E-06	Animation every 600 time step.	
24	9	3	0.005	0.6	18	3600	5000	5.00E-06	Animation every 600 time step.	
25	7	3	0.005	0.6	18	3600	5000	5.00E-06		
26	8	3	0.005	0.6	18	3600	5000	5.00E-06		
27	Validation	3	0.034	0.088	132	3883	5000	5.00E-06		
28	9	3	0.005	0.6	18	3600	5000	5.00E-06		
29	3	3	0.005	0.6	18	3600	5000	5.00E-06	Double viscosity	
30	3	3	0.005	0.6	312	62400	5000	5.00E-06	Psudo steady state	
31	ParticlesTest	3	0.005	0.6	18	3600	5000	5.00E-06	Wrong particle number. Only a test	

Table continued from previous page

32	ParticlesTest	3	0.005	0.6	18	3600	5000	5.00E-06	Wrong #particles = 29e6 Constant-number = 139. TFR = 0.18 Standard parcel release method.	

33	ParticlesTest	3	0.005	0.6	18	3600	5000	5.00E-06	TFR=640.
									#particles = 4.7e12.
									parcels = 172800.
									total mass = 1.1e4
									Standard parcel
									release method	

34	ParticlesTest	3	0.005	0.6	18	3600	5000	5.00E-06	TFR 3.704e-3.
									#particles =2.8e7.
									parcels = 172800.
									total mass = 0.067
									Standard parcel
									release method	

35	ParticlesTest	3	0.005	0.6	18	3600	5000	5.00E-06	TFR 1.23e-3.
									#particles =9.2e6.
									parcels = 172800.
									total mass = 2.2e-2
									Initialized by
									the solution at
									3600 iterations
									form Sim35	

36	ParticlesTest	3	0.005	0	327	65400	5000	5.00E-06	Two-way coupled simulations with #diameters=10. One particle per parcel and TFR=0.177944	71:48:00
37	ParticlesTest	3	0.005	0.6	7.305	1461	5000	5.00E-06		

Table continued from previous page

38	ParticlesTest	3	0.005	0.6	7.305	1461	5000	5.00E-06	One-way coupled simulations with #diameters=10. One particle per parcel and TFR=0.177945	08:10:00
39	Two-phase of particles	3	0.005	0.6	18	3600	5000	5.00E-06	One-way coupled simulations with #diameters=10. Standard injection model for particles TFR=0.177946. Two-phase particle injection	
40	Recirculation pump with particles	3	0.005	0.6	243	48530	5000	5.00E-06	One-way coupled simulations with #diameters=10. Standard injection model for particles TFR=0.177946. One-phase particle injection	
41	Particle simulation	3	0.005	0.6	18	3600	5000	5.00E-06	One-way coupled. one-phase with standrad injection	
42	Particle simulation	3	0.005	0.6	18	3600	5000	5.00E-06	One-way coupled. one-phase with standrad injection. Random walk model	

Table continued from previous page

43	Particle simulation	3	0.005	0.6	18	3600	5000	5.00E-06	One-way coupled. one-phase with standrad injection. DPM pressure gradient force and viritual mass force	07:00:00
44	Case 1 with particles	3	0.03	0.1	108	3600	5000	5.00E-06	One-way coupled. one-phase with standrad injection. DPM pressure gradient force and viritual mass force	
45	Particle simulation	3	0.005	0.6	18	3600	5000	5.00E-06	One-way coupled. one-phase with standrad injection. DPM pressure gradient force and viritual mass force. TFR = 0.2829 and	07:00:00

B Recirculation pump snapshots of particles in TR

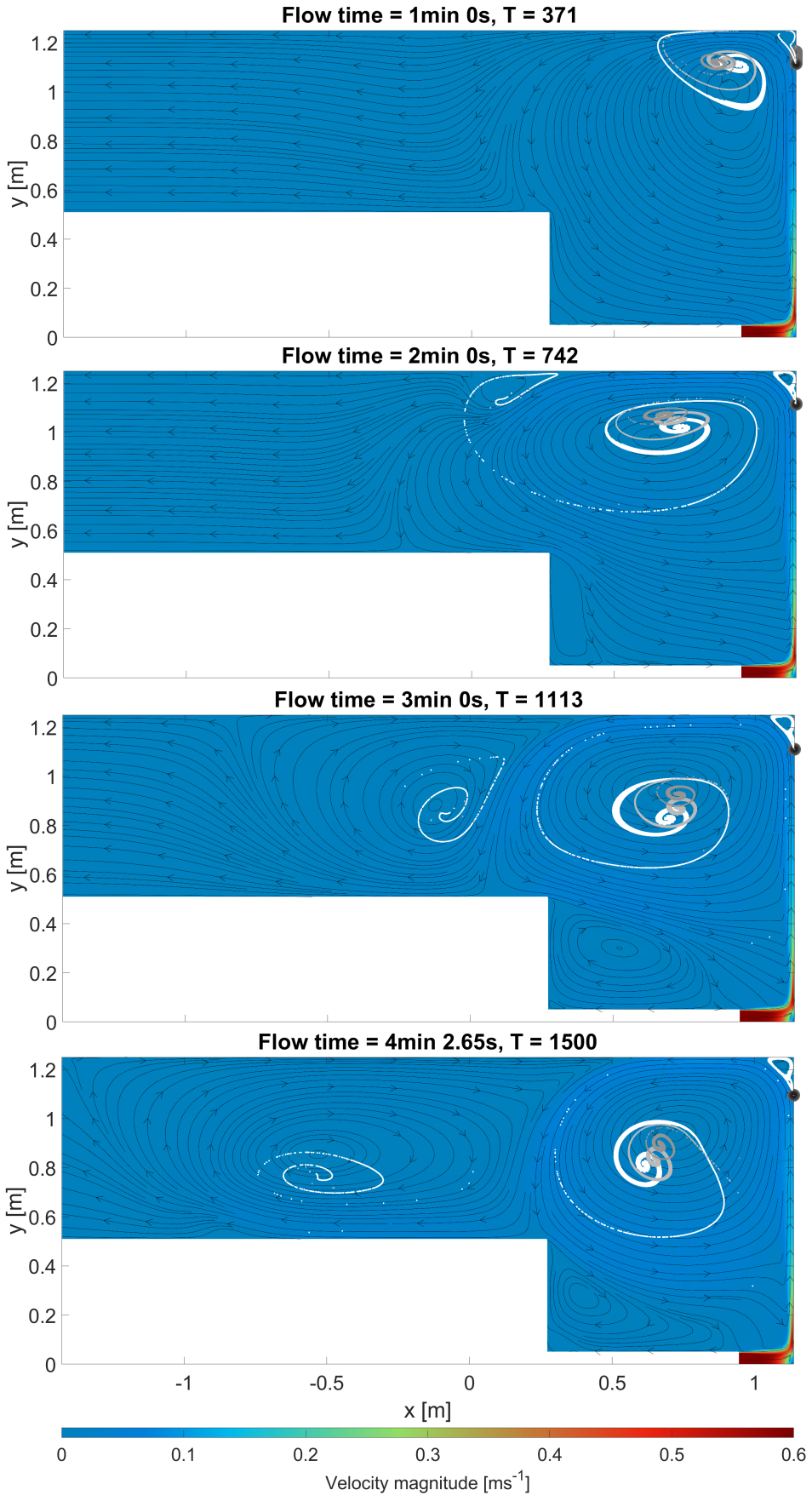

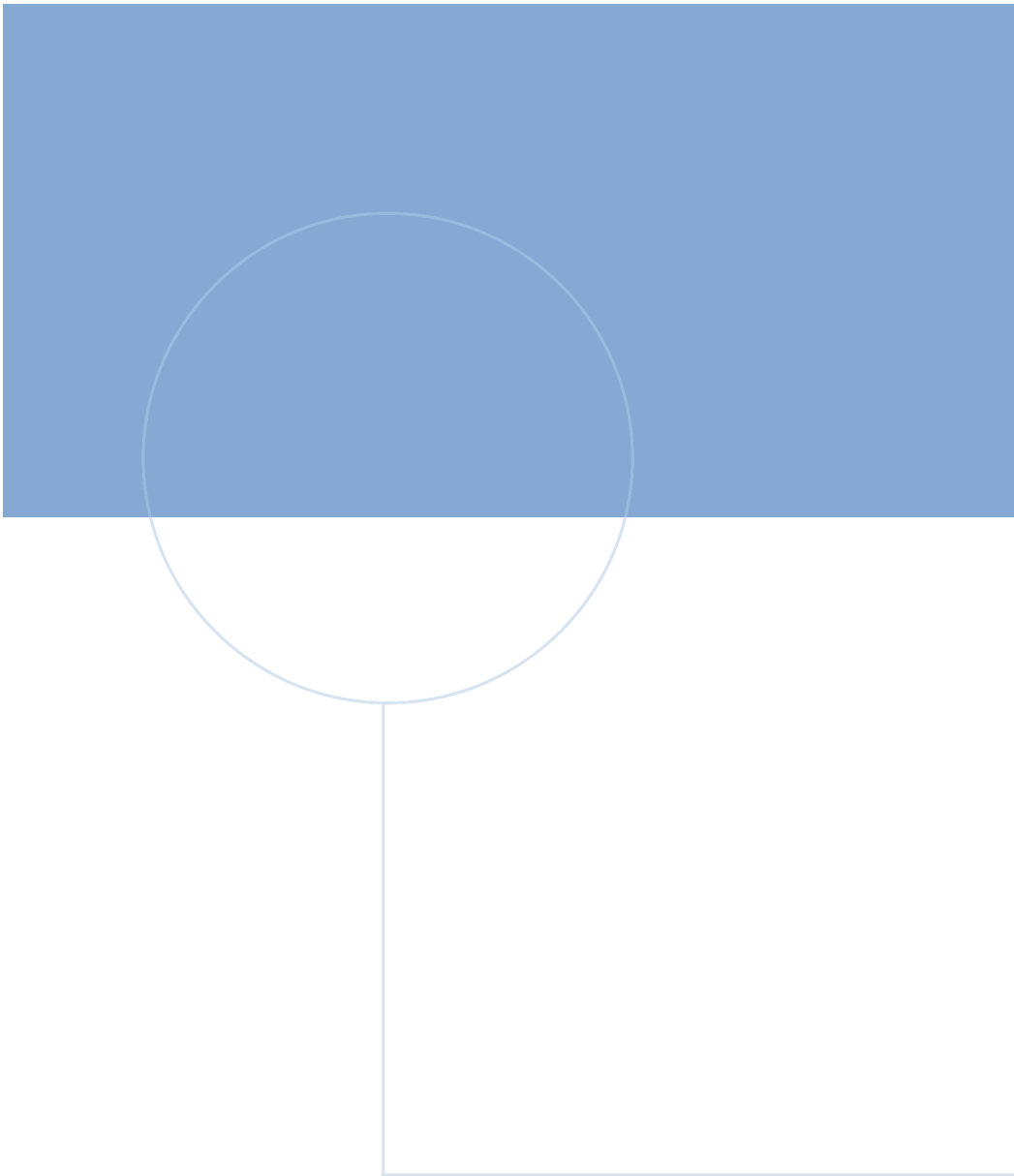

NTNU
Norwegian University of
Science and Technology

TELEMARK
TECHNOLOGIES™